THE ASTROPHYSICAL JOURNAL, 362:503–521, 1990 October 20

EXTRAGALACTIC GLOBULAR CLUSTERS. I. THE METALLICITY CALIBRATION[1]

JEAN P. BRODIE
Lick Observatory, University of California, Santa Cruz

AND

JOHN P. HUCHRA
Harvard-Smithsonian Center for Astrophysics
Received 1990 February 6; accepted 1990 April 18

ABSTRACT

We have explored the ability of absorption-line strength indices, measured from integrated globular cluster spectra, to predict mean cluster metallicity. Using statistical criteria, we have identified the six best indices out of ~20 measured in a large sample of Galactic and M31 cluster spectra. Linear relations between index and metallicity have been derived along with new calibrations of infrared colors ($V-K$, $J-K$, and CO) versus [Fe/H]. Estimates of metallicity from the six spectroscopic index–metallicity relations have been combined in three different ways to identify the most efficient estimator and the minimum bias estimator of [Fe/H]—the weighted mean. This provides an estimate of [Fe/H] accurate to about 15%.

Cyanogen at 4170 Å correlates with metallicity, but there is a significant offset between Galactic and M31 clusters which may be due to an abundance anomaly. Reddenings for individual M31 clusters can be estimated to an accuracy of about 0.04 in $E(B-V)$ by comparing metallicities derived from line-strength indices with those derived from infrared colors.

Subject headings: clusters: globular — galaxies: stellar content — stars: abundances

I. INTRODUCTION

The study of extragalactic globular clusters yields valuable information in a variety of astronomical contexts. Generally, their extreme age and compactness make them powerful probes of both the formation and the current dynamical state of galaxy halos. One fundamental problem is to determine to what extent globular cluster properties are universal and to what extent they depend on characteristics of the parent galaxy. This problem relates to our understanding of the early dynamical and chemical history of galaxies.

We now known that individual globular clusters span a wide range of age and spectral type, although for the well-studied cluster systems the high end of the range of metallicities has generally not exceeded solar. Certain properties of globular clusters can be loosely correlated with parent galaxy type. For example, irregular galaxies like the Magellanic Clouds (Searle, Wilkinson, and Bagnuolo 1980; Cohen 1981; Rabin 1982) and the Scd galaxy M33 (Christian and Schommer 1983) contain populous young blue clusters in addition to the normal old red clusters we find in our own Galaxy and Andromeda.

It has been generally assumed (e.g., Faber 1973) that old, red globular clusters have ages similar to the stars in elliptical galaxies and that the two stellar populations differ only in metal abundance. Burstein *et al.* (1981; 1984, hereafter BFGK) have challenged this view and suggest that anomalies in the strengths of certain absorption features in integrated cluster spectra point to the existence of more than one distinguishing physical parameter. BFGK claim that clusters in Andromeda have stronger Hβ and cyanogen (~4170 Å) absorption than Galactic globulars of the same metallicity (Mg2 strength). Andromeda clusters and elliptical galaxies seem to form a continuous distribution in the Hβ–Mg2 plane, with Galactic globulars falling below this relation. In the CN–Mg2 plane they find that Galactic clusters and the elliptical galaxies are continuous, while the Andromeda clusters have anomalously high CN. Tripicco (1989) has since confirmed that metal-rich Andromeda clusters exhibit anomalously strong CN for their spectral types.

A standard problem in the study of composite systems is that of defining precisely what is meant by the term "metallicity." Ideally, detailed comparisons of individual stars can be made with model stellar atmospheres. For most extragalactic systems one does not have this luxury.

We have identified a set of features in the integrated spectra of late-type stellar systems which appear to be sensitive to changes in the mean chemical abundance. The indices which measure the strengths of these features are combined to provide an estimate of the "mean metallicity" which will allow us to intercompare the global abundance characteristics of various extragalactic systems. We will refer to the mean metallicity as [Fe/H], the logarithmic ratio of metal abundance to the solar metal abundance, but stress that this term is applied loosely. Some of the indices do not, of course, measure the abundance of iron peak elements directly, but it is to be hoped that an estimate of [Fe/H] derived from several spectral features will be less sensitive to the kind of anomalies referred to above as well as to other systematic effects. Note that individual element abundances can, in principle, be investigated using our index measurements, and we will pursue this further in a later paper (Brodie and Huchra 1990).

In this paper we investigate a variety of metallicity-sensitive line-strength indices in Andromeda and Galactic globulars. We derive relations between metallicity and various line indices using Galactic globular clusters as calibrators. We then use these relations to derive metallicities for the Andromeda globular clusters. Frogel, Persson, and Cohen (1980) derive relationships between $V-K$ color and metallicity for Galactic globular clusters based on the Zinn (1980*a*) metallicity scale.

[1] Work reported here is based on observations made with the Multiple Mirror Telescope, a joint facility of the Smithsonian Institution and the University of Arizona.

We rederive this relationship using the revised metallicity scale of Zinn and West (1984), and derive new relationships between both the $J-K$ color and the infrared CO index and metallicity. These indices are used to estimate metallicities from published Andromeda cluster colors. We compare the metallicities derived from line strengths and from the infrared colors for the Adromeda clusters. We compare our line index measurements with those of BFGK, and we compare the abundance characteristics of the Galactic and Andromeda globular cluster systems.

In § II we describe the observations. In § III we describe the calibration of [Fe/H] versus index, and in § IV we discuss our results.

II. OBSERVATIONS

a) *Line Indices*

Various workers in the field have defined line indices to be used as metallicity and temperature indicators in integrated cluster spectra. Table 1 lists the standard bandpasses that have been used to define the indices and colors that various workers have measured. As explained below, not all of these are used in our metallicity calibrations. We provide the complete set here for easy reference. DDO indices were originally defined in terms of intermediate-band filters (McClure 1970). We have listed the corresponding bandwidths in Table 1 but note that pseudo-DDO indices measured from spectra are not directly comparable to photometric indices without a transformation. We treat the DDO indices separately in an appendix. The photometric Q_{39} index (Zinn 1980*a*) has not been included because it is not a spectroscopic index. It is the basis of the (Zinn and West 1984) metallicity scale we have adopted.

The majority of the standard bandpasses have been described by Faber and Burstein (Faber 1973; BFGK), Brodie and Hanes (1986), and Suntzeff (1980, 1981). The elements and molecules whose features are most commonly measured are calcium, sodium, magnesium, iron, hydrogen cyanogen, titanium oxide, magnesium hydride, and CH. The strongest features in the integrated spectra of late-type systems, and thus the easiest to measure, are the line-blanketing discontinuity at 4000 Å, the H and K lines of Ca II, the CN and CH (G band) features, the magnesium *b* triplet, the magnesium hydride trough, and the sodium D doublet. Iron lines and the Balmer lines are generally weaker features in these spectra. As defined, many of the index bandpasses include not just the nominal feature but also contributions from other elements with absorption lines in the same region of the spectrum. An example of a spectrum of an object dominated by a late-type stellar population is shown in Figure 1.

TABLE 1

DEFINITIONS FOR LINE INDICES AND COLORS

Index	*C*1	*I*	*C*2
Suntzeff			
CA	3650.00–3780.0	3910.00–4020.00	4020.00–4130.00
HK	...	3910.00–4020.00	4020.00–4130.00
CN	...	3850.00–3878.00	3896.00–3912.00
Faber and Burstein			
*CNR	4082.00–4118.50	4144.00–4177.50	4246.00–4284.75
*CH = G band	4268.25–4283.25	4283.25–4317.00	4320.75–4335.75
*Hβ	4829.50–4848.25	4849.50–4877.00	4878.25–4892.00
*MgH	4897.00–4958.25	5071.00–5134.75	5303.00–5366.75
*Mg2	4897.00–4958.25	5156.00–5197.25	5303.00–5366.75
*Mgb	5144.50–5162.00	5162.00–5193.25	5193.25–5207.00
*Fe 5270 = FE52	5235.50–5249.25	5248.00–5286.75	5288.00–5319.25
Fe 5335	5307.25–5317.25	5314.75–5353.50	5356.00–5364.75
*Na I	5863.00–5876.75	5879.25–5910.50	5924.50–5949.25
TiO 1	5819.00–5850.25	5939.00–5995.25	6041.00–6104.75
TiO 2	6069.00–6142.75	6192.00–6273.25	6375.00–6416.25
Brodie and Hanes			
*CNB	3785.00–3810.00	3810.00–3910.00	3910.00–3925.00
*H+K	3910.00–3925.00	3925.00–3995.00	3995.00–4010.00
Ca I	4200.00–4215.00	4215.00–4245.00	4245.00–4260.00
G	4275.00–4285.00	4285.00–4315.00	4315.00–4325.00
Hb	4800.00–4830.00	4830.00–4890.00	4890.00–4920.00
*MgG	5125.00–5150.00	5150.00–5195.00	5195.00–5220.00
MH	4740.00–4940.00	4940.00–5350.00	5350.00–5550.00
FC	5225.00–5250.00	5250.00–5280.00	5280.00–5305.00
Na D	5835.00–5865.00	5865.00–5920.00	5920.00–5950.00
*Δ	3800.00–4000.00	4000.00–4200.00	...
DDO			
C3842	3707.00–3808.00	4214.00–4297.00	
C3841	3707.00–3808.00	4123.00–4207.00	
C4245	4214.00–4297.00	4476.00–4559.00	
C4142	4123.00–4207.00	4214.00–4297.00	
C4548	4476.00–4559.00	4879.00–4974.00	

NOTE.—Asterisks indicate indices discussed in this paper.

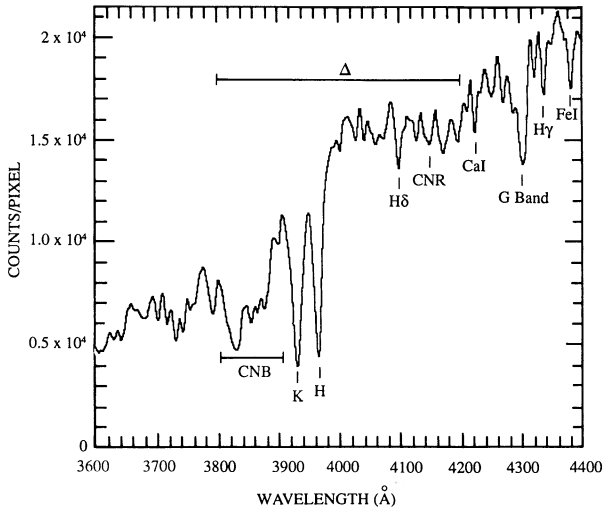

FIG. 1a

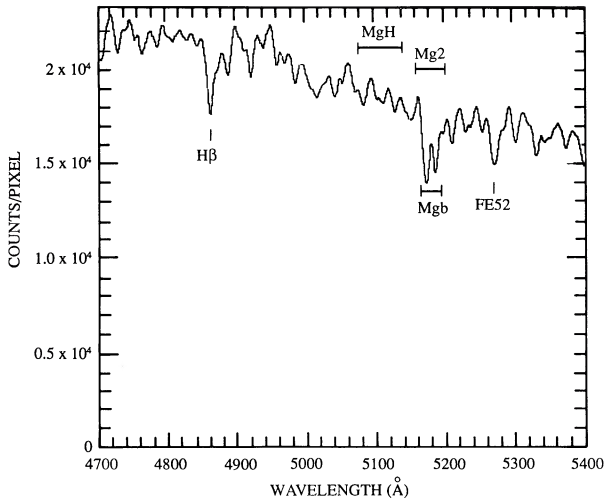

FIG. 1b

FIG. 1.—High signal-to-noise spectrum of the M31 globular cluster 225–280 with various spectral features marked in the wavebands (*a*) 3600–4400 Å and (*b*) 4700–5400 Å.

We define all of the indices in terms of line magnitudes derived from mean flux ratios between continuum bandpasses and the feature bandpass:

$$F_B = \int_{\lambda_1}^{\lambda_2} F_\lambda \, d\lambda/(\lambda_2 - \lambda_1) \tag{1}$$

is the mean flux (in ergs s^{-1} cm^{-2} $Å^{-1}$) in band B;

$$I = -2.5 \log \left[\frac{2F_I}{F_{C1} + F_{C2)}} \right] \tag{2}$$

is the feature index, and F_{C1} and F_{C2} are the mean fluxes in the continuum bandpasses and F_I the mean flux in the feature. Those indices which are simple colors are defined as

$$I = -2.5 \log (F_2/F_1) . \tag{3}$$

Note that feature indices can be converted into equivalent widths, W_λ (and vice versa), by the relation

$$W_\lambda(I) = (\lambda_2 - \lambda_1)(1 - 10^{-I/2.5}) , \tag{4}$$

where λ_2 and λ_1 are the maximum and minimum wavelengths defining the *feature* bandpass.

Note also that it is *absolutely essential* that the bandpass be shifted to account for the radial velocity of the object. For example, the Andromeda globular cluster system has a velocity dispersion of almost 150 km s^{-1}, which translates into a range of over 600 km s^{-1}, or a shift of 8 Å at 4000 Å. This is 25% of the width of many of the feature bandpasses listed in Table 1. In addition, although none of the objects in our current studies require it, at large redshift it is necessary to correct the line indices and equivalent widths as defined above to the rest frame by multiplying by a factor of $1+z$.

We have computed all of the indices listed in Table 1 from both flat-fielded spectra that have been converted to F_λ (by means of Oke and Stone standard stars and mean extinction coefficients) and flat-fielded spectra left in pixel space. The feature indices computed in these different ways are the same to within a few percent in all cases. Color indices are, of course, quite different. The computation in pixel space allows us to estimate the photon statistical (internal) errors in the indices and colors;

$$\sigma_B = \frac{[Q + 2(S + D)]^{1/2}}{Q} , \tag{5}$$

is the fractional statistical error in the flux in bandpass B, where O, S, and D are the total accumulated counts in the bandpass in the object, sky, and dark, respectively. The photon statistical error in the index is then the quadrature

$$\sigma_P = (\sigma_{C1}^2 + \sigma_L^2 + \sigma_{C2}^2)^{1/2} , \tag{6}$$

where σ_L, σ_{C1}, and σ_{C2} refer to the statistical error in the line and adjacent continuum bandpasses. The statistical error in any color is the quadrature of the error in just two bandpasses. For the case of a combination of multiple spectra of a single object, a weighted average is given with the internal error, σ_{MM}, computed as the reduced quadrature of the photometric errors of the individual spectra in the average,

$$\sigma_{MM} = \left(\sum_i \frac{1}{\sigma_{Pi}^2} \right)^{-1/2} . \tag{7}$$

Many of the indices listed in Table 1 are measures of the same features. For example, Suntzeff's CA index and the Brodie and Hanes H+K index are both measures of the strength of the Ca H and K lines. The Faber and Burstein MgH and the Brodie and Hanes MH are both measures of the magnesium hydride strength. Both the Faber and Burstein Mg2 and Mgb indices and the Brodie and Hanes MgG index (this was originally also called Mgb but has been renamed MgG here to avoid confusion with the Faber and Burstein index) are measures of the magnesium *b* triplet. The main difference between similar indices is usually in the choice of the continuum bandpasses. In general the continuum level in these late-type objects is difficult to define owing to the presence of large numbers of weak and intermediate-strength lines of many different chemical elements.

In what follows we study the behavior of 12 of the indices listed in Table 1. These 12 are marked with asterisks in the table. The selection criteria were as follows. Where two or more indices measured the same feature, only one was selected

by us. For most features the Faber and Burstein index was chosen because theirs is the largest data base in the literature of measurements of Galactic globulars, M31 globulars, galaxies, and individual giant stars. We studied all three of the magnesium indices (Mg2, Mgb, and MgG) to examine the effects of the slightly different bandpasses and different choices of continuum bands and to determine the best metallicity indicator. Our measurements of the TiO indices have not been presented here because of the possibility of second-order contamination in this region of the MMT spectra. Brodie and Hanes indices were selected in favor of Suntzeff indices, again because of data base considerations. The 12 indices selected measure a variety of chemical elements and cover a broad region of the spectrum. These factors deserve serious consideration in establishing a method of metallicity determination which is as insensitive as possible to abundance anomalies and observational errors.

b) *MMT Observations*

We and our collaborators have observed a large number of globular cluster candidates around several galaxies with the MMT spectrograph. In addition, observations have been made of bright galaxies, individual stars in Galactic globular clusters and in Local Group dwarf galaxies, and also of Virgo Cluster dwarf galaxies (from the lists of Caldwell 1983 and Binggeli, Sandage, and Tammann 1985). Most of these observations were made primarily to obtain radial velocities. For the faintest objects the spectra are of low signal-to-noise ratio and thus will produce only poor line indices for abundance work. For the brighter objects, especially the Andromeda globulars and the Galactic globular cluster stars, care was taken to obtain higher signal-to-noise spectra. Here we will discuss the observations of the Andromeda globular cluster system and calibrating objects in our own Galaxy. Observations of the other systems will be described in subsequent papers. The complete and extensive data set will be presented in an associated *Astrophysical Journal Supplement* paper (Huchra, Brodie, and Stauffer 1991, hereafter HBS).

The initial set of Andromeda cluster observations at the MMT (Huchra, Stauffer, and van Speybroeck 1982) were made with a photon-counting Reticon behind a three stage Varo image tube on the MMT spectrograph. A 300 line mm^{-1} grating was used which produced spectra with a resolution of 5–6 Å and spectral coverage of 3800–6500 Å. The front photocathode was an S25, and the sensitivity rolled off significantly below 4300 Å. Additional observations of Andromeda globular clusters and other systems have been obtained with the MMT during a dozen observing runs over the last several years. Most of the new data were taken with the same basic system but using an S20 magnetically focused EMI image tube (Cromwell and Weymann 1982) with a fiber optic reducing boule between the image tube and the Reticon (Latham 1982). This system has slightly poorer resolution (8–9 Å) but considerably enhanced blue sensitivity. The new observations extend to the atmospheric cutoff at 3200 Å. This is important because many of the strongest and most metallicity-sensitive features are in the UV. Many objects that were observed initially with the red system have also been reobserved with the blue system in order to provide a sample with homogeneous wavelength coverage.

Table 2 contains the indices for objects in the sample we will discuss here (including the averaged indices for those objects with multiple observations). In Table 2 the first line is the index and the second line is the 1 σ internal statistical error in the measurement from the photon statistics. Please note that these errors do not include the systematic errors which we will discuss below. Errors are shown where they have been computed by us. Otherwise the errors may be found in the literature.

For a small number (18) of bright Andromeda globular clusters in common with the study of Burstein *et al.* (1984) we have also obtained higher resolution, high signal-to-noise observations with an 832 line mm^{-1} grating and the MMT spectrograph. These observations have a resolution of 1.5–2.0 Å and cover 4750–5450 Å.

c) *Lick and AAT Observations*

Certain indices were measured for Galactic globular clusters and are also given in Table 2. These measurements are taken from Brodie and Hanes (1986) and are based on observations made at Lick Observatory and at the Anglo-Australian Observatory. Full observational details are given in Brodie and Hanes (1986), but we briefly summarize them here.

The Mark 1 Robinson-Wampler scanner was used on the Lick Observatory 61 cm telescope to acquire spectra at roughly 12 Å resolution of the integrated light of 24 Galactic globular clusters. Total integration times were typically 3600 s per cluster, and during the integrations the telescope was occasionally stepped a few arcseconds perpendicular to the long axis of the slit in order to sample a representative mix of cluster stars.

The Image Photon Counting System (IPCS) was used on the 3.9 m Anglo-Australian telescope (AAT) to acquire spectra at roughly 5 Å resolution of 17 Galactic globular clusters. The telescope was nodded perpendicular to the long slit and typically through 30″ sweeps over the face of each cluster to yield a spectrum of the integrated light.

Overlap between the Lick and AAT samples yields indices for a total of 36 Galactic globulars. The indices found in Brodie and Hanes (1986), I_{BH}, can be converted to our line-magnitude system via

$$I = -2.5 \log (1 - I_{BH}) . \quad (8)$$

Note that their Δ index is already defined as a magnitude and need not be converted.

d) *Observation from Other Sources*

A substantial number of high-quality spectra of both Galactic and Andromeda globular clusters and individual K giant stars have also been obtained by BFGK. BFGK define indices in two different ways. The equivalent widths in BFGK have been converted into line magnitudes via the inverse relation of equation (4):

$$I = -2.5 \log \left(1 - \frac{W_\lambda}{\lambda_2 - \lambda_1}\right) . \quad (9)$$

BFGK's line magnitudes are defined in exactly the same way as ours.

Figure 2 shows the comparison of our measurements of several of the important line indices and those of BFGK for the 34 objects we have in common. Table 3 gives the mean difference and the sigma of our measurements compared with those of BFGK. In general, there is excellent agreement between the two sets of measurements, with near unity slopes and negligible (at the 1% level) offsets. The $\sim$0.02 offset for Mg2 is probably systematic, but such problems are not unexpected in a comparison of data taken at different telescopes with different

TABLE 2

LINE INDICES

Name (1)	Δ (2)	HK (3)	CNB (4)	CNR (5)	CH (6)	Hβ (7)	Mg2 (8)	MgH (9)	Mgb (10)	MgG (11)	FE52 (12)	Na I (13)
NGC 1851	0.348	0.254	0.079	...	...	...	...	...	...	0.027	...	...
	0.006	0.010	0.011	...	...	...	...	...	...	0.009	...	...
NGC 1904	0.213	0.178	0.041	...	...	...	...	...	...	0.006	...	...
	0.004	0.007	0.007	...	...	...	...	...	...	0.009	...	...
NGC 2298	0.177	0.182	0.049	...	...	...	...	...	...	0.055	...	...
	0.011	0.021	0.021	...	...	...	...	...	...	0.020	...	...
NGC 5024	0.152	0.125	−0.018	−0.127	0.037	0.114	0.039	0.002	0.025	0.005	0.018	0.017
	0.013	0.023	0.023	0.023	0.021	0.012	0.015	0.011	0.006	0.016	0.010	0.013
NGC 5272	0.222	0.151	0.011	−0.079	0.075	0.101	0.042	−0.002	0.027	0.012	0.033	0.038
	0.006	0.010	0.010	0.012	0.011	0.006	0.008	0.006	0.004	0.009	0.005	0.007
NGC 5634	0.229	0.164	−0.006	...	...	...	...	...	...	0.013	...	...
	0.015	0.026	0.026	...	...	...	...	...	...	0.019	...	...
NGC 5904	0.290	0.200	0.051	−0.085	0.072	0.094	0.064	0.012	0.037	0.025	0.034	0.041
	0.004	0.006	0.006	0.008	0.008	0.004	0.006	0.004	0.003	0.007	0.004	0.005
NGC 5927	0.577	0.282	0.214	...	...	...	...	...	...	0.117	...	...
	0.010	0.017	0.020	...	...	...	...	...	...	0.010	...	...
NGC 5946	0.288	0.240	0.037	...	...	...	...	...	...	0.022	...	...
	0.007	0.013	0.014	...	...	...	...	...	...	0.009	...	...
NGC 5986	0.253	0.213	0.048	...	...	...	...	...	...	0.031	...	...
	0.005	0.009	0.009	...	...	...	...	...	...	0.008	...	...
NGC 6093	0.203	0.162	0.016	...	...	...	...	...	...	0.014	...	...
	0.007	0.012	0.012	...	...	...	...	...	...	0.010	...	...
NGC 6171	0.433	0.249	0.121	−0.107	0.118	0.060	0.106	0.021	0.066	0.037	0.056	0.066
	0.016	0.030	0.030	0.020	0.019	0.011	0.013	0.010	0.007	0.020	0.008	0.012
NGC 6205	0.248	0.185	0.054	−0.085	0.061	0.093	0.043	0.001	0.027	0.010	0.027	0.037
	0.010	0.017	0.017	0.006	0.006	0.003	0.004	0.003	0.002	0.013	0.003	0.004
NGC 6218	0.293	0.154	0.062	−0.096	0.075	0.106	0.071	0.011	0.051	0.028	0.033	0.050
	0.016	0.029	0.029	0.013	0.012	0.007	0.009	0.006	0.005	0.019	0.005	0.008
NGC 6229	0.296	0.201	0.037	−0.094	0.062	0.085	0.084	0.012	0.048	0.027	0.029	0.040
	0.014	0.025	0.025	0.023	0.021	0.012	0.015	0.011	0.008	0.017	0.010	0.013
NGC 6254	0.223	0.155	0.064	...	...	...	...	...	...	0.019	...	...
	0.015	0.026	0.026	...	...	...	...	...	...	0.018	...	...
NGC 6273	0.253	0.163	0.001	...	...	...	...	...	...	0.011	...	...
	0.015	0.026	0.026	...	...	...	...	...	...	0.018	...	...
NGC 6341	0.173	0.129	0.002	−0.099	0.016	0.107	0.013	−0.012	0.024	0.015	0.007	0.033
	0.010	0.018	0.018	0.007	0.007	0.004	0.005	0.003	0.002	0.013	0.003	0.004
NGC 6352	0.526	0.244	0.124	...	...	...	...	...	...	0.070	...	...
	0.013	0.024	0.027	...	...	...	...	...	...	0.017	...	...
NGC 6356	0.566	0.317	0.194	0.015	0.156	0.060	0.174	0.058	0.109	0.065	0.058	0.117
	0.006	0.011	0.012	0.017	0.016	0.010	0.010	0.008	0.006	0.008	0.007	0.010
NGC 6362	0.421	0.250	0.108	...	...	...	...	...	...	0.062	...	...
	0.017	0.030	0.033	...	...	...	...	...	...	0.020	...	...
NGC 6402	0.309	0.154	0.013	...	...	...	...	...	...	0.015	...	...
	0.016	0.029	0.029	...	...	...	...	...	...	0.019	...	...
NGC 6541	0.221	0.200	0.045	...	...	...	...	...	...	0.024	...	...
	0.004	0.006	0.006	...	...	...	...	...	...	0.007	...	...
NGC 6624	...	...	...	0.020	0.165	0.071	0.154	0.053	0.095	...	0.063	0.105
	...	...	...	0.013	0.012	0.007	0.009	0.006	0.005	...	0.003	0.008
NGC 6626	0.356	0.201	0.057	...	...	...	...	...	...	0.032	...	...
	0.013	0.023	0.023	...	...	...	...	...	...	0.016	...	...
NGC 6637	...	...	...	−0.008	0.180	0.046	0.134	0.045	0.079	...	0.061	0.113
	...	...	...	0.018	0.017	0.010	0.012	0.009	0.006	...	0.011	0.004
NGC 6712	0.398	0.243	0.127	−0.053	0.086	0.074	0.110	0.054	0.056	0.073	0.041	0.149
	0.008	0.016	0.017	0.013	0.013	0.007	0.009	0.007	0.005	0.011	0.006	0.008
NGC 6723	0.339	0.222	0.069	...	...	...	...	...	...	0.038	...	...
	0.007	0.013	0.013	...	...	...	...	...	...	0.015	...	...
NGC 6752	0.231	0.222	0.074	...	...	...	...	...	...	0.051	...	...
	0.004	0.008	0.008	...	...	...	...	...	...	0.010	...	...
NGC 6779	0.226	0.186	0.041	...	...	...	...	...	...	0.011	...	...
	0.016	0.029	0.029	...	...	...	...	...	...	0.019	...	...
NGC 6809	0.131	0.177	0.029	...	...	...	...	...	...	0.026	...	...
	0.008	0.014	0.014	...	...	...	...	...	...	0.019	...	...
NGC 6838	0.540	0.281	0.113	−0.017	0.182	0.058	0.128	0.052	0.082	0.111	0.042	0.069
	0.012	0.023	0.025	0.026	0.024	0.014	0.018	0.013	0.009	0.014	0.011	0.015
NGC 6864	0.332	0.252	0.072	...	...	...	...	...	...	0.038	...	...
	0.005	0.010	0.010	...	...	...	...	...	...	0.010	...	...
NGC 6934	0.274	0.184	0.028	...	...	...	...	...	...	0.032	...	...
	0.015	0.026	0.026	...	...	...	...	...	...	0.018	...	...
NGC 6981	0.273	0.212	0.038	−0.069	0.032	0.096	0.050	0.014	0.025	0.029	0.024	0.055
	0.007	0.013	0.013	0.020	0.019	0.011	0.014	0.010	0.007	0.013	0.008	0.012
NGC 7006	0.248	0.197	−0.023	−0.054	0.114	0.098	0.059	0.034	0.016	0.011	0.014	0.064
	0.017	0.030	0.030	0.024	0.022	0.013	0.016	0.012	0.008	0.029	0.010	0.014

TABLE 2—*Continued*

Name (1)	Δ (2)	HK (3)	CNB (4)	CNR (5)	CH (6)	Hβ (7)	Mg2 (8)	MgH (9)	Mgb (10)	MgG (11)	Fe52 (12)	NaI (13)
NGC 7078	0.175	0.114	−0.013	−0.102	0.222	0.105	0.017	−0.005	0.011	0.015	0.028	0.067
	0.008	0.014	0.014	0.010	0.009	0.005	0.007	0.002	0.004	0.011	0.004	0.006
NGC 7089	0.243	0.150	0.008	−0.079	0.057	0.106	0.052	0.002	0.031	0.020	0.031	0.045
	0.011	0.019	0.019	0.008	0.007	0.004	0.005	0.004	0.003	0.014	0.003	0.005
000–001	0.468	0.303	0.111	0.051	0.120	0.056	0.108	0.042	0.075	0.057	0.043	0.062
	0.007	0.023	0.026	0.011	0.014	0.009	0.006	0.006	0.011	0.009	0.009	0.013
000–33	0.170	0.172	0.026	−0.005	0.069	0.063	0.030	0.021	0.044	0.040	0.025	0.096
	0.012	0.041	0.042	0.018	0.022	0.018	0.011	0.010	0.017	0.014	0.016	0.022
6–58	0.523	0.322	0.198	0.071	0.174	0.065	0.187	0.056	0.143	0.098	0.076	0.139
	0.008	0.027	0.029	0.018	0.024	0.022	0.015	0.013	0.024	0.020	0.022	0.031
12–64	0.111	0.226	0.088	−0.047	0.077	0.101	0.041	−0.015	0.048	0.036	−0.003	0.049
	0.007	0.023	0.023	0.013	0.017	0.014	0.009	0.008	0.015	0.012	0.013	0.018
19–72	0.475	0.248	0.039	0.039	0.108	0.131	0.099	0.042	0.080	0.058	0.050	0.098
	0.012	0.038	0.044	0.019	0.023	0.017	0.011	0.010	0.017	0.014	0.015	0.022
20–73	0.375	0.306	0.137	0.023	0.118	0.093	0.119	0.041	0.079	0.042	0.058	0.082
	0.006	0.016	0.021	0.010	0.013	0.011	0.007	0.006	0.012	0.010	0.011	0.014
000–76	0.313	0.268	0.060	0.030	0.106	0.093	0.085	0.030	0.045	0.038	0.033	0.068
	0.007	0.026	0.028	0.011	0.013	0.009	0.006	0.006	0.010	0.008	0.009	0.012
58–119	0.204	0.289	0.109	0.001	0.108	0.098	0.102	0.015	0.088	0.055	0.013	0.061
	0.006	0.021	0.021	0.011	0.013	0.011	0.007	0.006	0.011	0.009	0.010	0.014
000–127	0.346	0.299	0.101	−0.018	0.133	0.146	0.129	0.021	0.066	0.065	0.063	0.025
	0.008	0.028	0.029	0.018	0.023	0.020	0.013	0.011	0.021	0.017	0.019	0.024
158–213	0.414	0.351	0.143	0.043	0.124	0.085	0.109	0.032	0.089	0.042	0.048	0.102
	0.003	0.008	0.009	0.005	0.007	0.006	0.004	0.003	0.007	0.005	0.006	0.008
163–217	0.602	0.383	0.273	0.135	0.147	0.082	0.201	0.069	0.169	0.103	0.107	0.161
	0.005	0.015	0.020	0.009	0.012	0.010	0.007	0.006	0.011	0.009	0.010	0.013
000–219	0.228	0.183	0.063	−0.068	0.053	0.129	0.019	−0.008	0.021	0.014	−0.001	−0.010
	0.008	0.028	0.029	0.015	0.019	0.017	0.011	0.010	0.018	0.014	0.017	0.024
171–222	0.690	0.359	0.283	0.114	0.136	0.055	0.168	0.076	0.125	0.069	0.066	0.140
	0.010	0.034	0.041	0.016	0.020	0.015	0.009	0.008	0.016	0.013	0.014	0.019
179–230	0.323	0.290	0.170	0.004	0.150	0.055	0.077	0.020	0.078	0.044	0.022	0.025
	0.011	0.039	0.040	0.018	0.022	0.018	0.011	0.010	0.018	0.014	0.016	0.021
182–233	0.476	0.305	0.136	−0.028	0.112	0.105	0.069	0.045	0.026	0.043	0.033	0.089
	0.011	0.040	0.043	0.019	0.024	0.018	0.011	0.010	0.019	0.015	0.017	0.022
193–244	0.605	0.258	0.261	0.126	0.151	0.069	0.197	0.069	0.150	0.086	0.107	0.135
	0.012	0.042	0.047	0.019	0.022	0.016	0.010	0.009	0.017	0.007	0.015	0.020
205–256	0.312	0.281	0.093	−0.034	0.110	0.076	0.082	0.031	0.074	0.038	0.024	0.053
	0.006	0.022	0.022	0.011	0.014	0.013	0.008	0.007	0.013	0.011	0.012	0.016
212–263	0.178	0.223	0.070	−0.055	0.054	0.095	0.042	0.004	0.056	0.028	0.017	0.073
	0.011	0.036	0.037	0.017	0.022	0.018	0.011	0.010	0.018	0.015	0.016	0.024
218–272	0.336	0.333	0.182	0.011	0.112	0.088	0.102	0.028	0.075	0.051	0.030	0.076
	0.005	0.014	0.019	0.010	0.013	0.013	0.008	0.007	0.014	0.011	0.012	0.016
224–279	0.215	0.283	0.058	−0.049	0.023	0.132	0.027	−0.013	0.045	0.021	0.001	0.022
	0.011	0.037	0.040	0.021	0.026	0.022	0.013	0.013	0.023	0.018	0.020	0.030
225–280	0.518	0.346	0.216	0.100	0.151	0.071	0.163	0.046	0.130	0.086	0.063	0.121
	0.001	0.004	0.004	0.002	0.003	0.003	0.002	0.002	0.003	0.003	0.003	0.004
240–302	0.174	0.257	0.058	−0.025	0.071	0.100	0.051	−0.003	0.015	0.039	−0.001	0.070
	0.008	0.028	0.030	0.015	0.019	0.016	0.010	0.009	0.016	0.013	0.014	0.020
NGC 188–Ave	0.908	0.326	0.277	0.261	0.225	0.051	0.240	0.103	0.133	0.083	0.116	0.147
	0.006	0.018	0.023	0.010	0.011	0.009	0.006	0.005	0.010	0.008	0.009	0.011
188 II-51	0.993	0.334	0.305	0.263	0.222	0.071	0.262	0.117	0.137	0.111	0.098	0.148
	0.014	0.045	0.060	0.023	0.027	0.022	0.014	0.012	0.023	0.019	0.020	0.025
188 II-76	0.876	0.376	0.421	0.262	0.196	0.044	0.174	0.056	0.130	0.054	0.044	0.119
	0.012	0.038	0.049	0.021	0.025	0.021	0.014	0.012	0.023	0.018	0.020	0.026
188 II-88	0.836	0.450	0.408	0.313	0.249	0.100	0.256	0.086	0.140	0.070	0.035	0.135
	0.027	0.077	0.110	0.043	0.047	0.033	0.022	0.019	0.037	0.030	0.031	0.039
188 I-57	0.967	0.367	0.399	0.256	0.149	0.056	0.217	0.097	0.140	0.096	0.125	0.174
	0.022	0.074	0.088	0.038	0.043	0.030	0.020	0.018	0.032	0.026	0.029	0.036
188 I-1	0.729	0.245	0.158	0.225	0.248	0.062	0.231	0.088	0.134	0.095	0.115	0.129
	0.010	0.033	0.040	0.019	0.023	0.019	0.013	0.011	0.021	0.017	0.018	0.024
188 II-72	1.133	0.337	0.229	0.287	0.245	0.021	0.276	0.144	0.128	0.077	0.146	0.102
	0.012	0.039	0.050	0.019	0.023	0.017	0.011	0.010	0.019	0.015	0.015	0.020
M92 IV114	0.294	0.220	0.008	−0.013	0.113	0.067	0.039	−0.018	0.012	0.031	0.076	0.074
	0.008	0.026	0.026	0.018	0.024	0.024	0.016	0.015	0.026	0.021	0.024	0.031
M92 III13	0.590	0.323	0.049	0.071	0.172	0.053	0.065	0.007	0.024	0.002	0.035	0.005
	0.008	0.027	0.029	0.017	0.022	0.018	0.012	0.011	0.020	0.016	0.018	0.021
M92 IX12	0.139	0.145	0.005	−0.068	0.087	0.144	0.055	−0.015	−0.006	0.003	0.008	0.023
	0.008	0.028	0.028	0.021	0.029	0.031	0.021	0.019	0.035	0.028	0.032	0.044
M92 XII8	0.389	0.242	−0.053	0.028	0.110	0.051	0.037	−0.008	0.006	0.015	0.001	0.003
	0.008	0.028	0.029	0.018	0.023	0.021	0.014	0.012	0.022	0.018	0.021	0.025
M3 IV25	0.744	0.337	0.142	0.049	0.225	0.046	0.030	−0.002	0.049	−0.007	0.058	0.036
	0.009	0.031	0.033	0.018	0.024	0.020	0.013	0.012	0.021	0.017	0.020	0.024
M3 III28	0.783	0.346	0.111	0.029	0.198	0.083	0.064	0.003	0.048	0.026	0.047	−0.002
	0.010	0.034	0.037	0.019	0.025	0.019	0.012	0.011	0.020	0.016	0.018	0.022

TABLE 2—*Continued*

Name (1)	Δ (2)	HK (3)	CNB (4)	CNR (5)	CH (6)	Hβ (7)	Mg2 (8)	MgH (9)	Mgb (10)	MgG (11)	Fe52 (12)	NaI (13)
M3 AV	0.696	0.402	0.160	0.034	0.246	0.046	0.033	−0.031	0.003	−0.001	0.061	0.058
	0.011	0.038	0.040	0.023	0.030	0.026	0.018	0.016	0.029	0.023	0.026	0.034
M5 IV86	0.226	0.221	−0.028	−0.041	0.065	0.107	0.048	−0.017	0.020	0.015	0.039	0.021
	0.004	0.015	0.015	0.011	0.014	0.015	0.010	0.009	0.017	0.013	0.016	0.023
M5 III3	1.019	0.361	0.037	0.101	0.239	0.042	0.137	0.060	0.057	0.024	0.050	0.054
	0.010	0.037	0.041	0.019	0.023	0.018	0.011	0.010	0.019	0.015	0.017	0.020
M5 IV19	1.061	0.418	0.139	0.070	0.211	0.046	0.124	0.064	0.078	0.035	0.030	0.065
	0.011	0.037	0.043	0.020	0.025	0.019	0.012	0.011	0.020	0.016	0.018	0.021
M5 II51	0.770	0.415	0.194	0.118	0.141	0.042	0.082	−0.011	0.067	0.042	0.037	0.058
	0.010	0.032	0.037	0.020	0.026	0.024	0.016	0.014	0.026	0.021	0.024	0.031
M5 IV59	1.002	0.350	0.154	0.169	0.258	0.106	0.083	0.028	0.026	0.021	0.040	0.053
	0.009	0.030	0.036	0.016	0.020	0.016	0.010	0.009	0.017	0.013	0.015	0.018
M13 786	0.961	0.335	0.105	0.185	0.212	0.068	0.062	0.011	0.042	0.025	0.094	0.039
	0.010	0.035	0.040	0.019	0.022	0.016	0.010	0.009	0.017	0.013	0.015	0.017
M13 818	0.302	0.328	0.067	0.034	0.110	0.016	0.062	−0.005	0.016	−0.013	0.081	0.021
	0.007	0.023	0.023	0.017	0.022	0.023	0.015	0.014	0.025	0.021	0.024	0.032
M71 A-7	0.990	0.430	0.296	0.289	0.234	0.066	0.220	0.104	0.129	0.089	0.059	0.128
	0.018	0.057	0.074	0.030	0.033	0.023	0.014	0.013	0.024	0.020	0.021	0.025
M71 A-6	1.194	0.388	0.051	0.170	0.172	0.012	0.314	0.205	0.121	0.105	0.114	0.155
	0.016	0.057	0.701	0.023	0.026	0.016	0.010	0.009	0.018	0.014	0.014	0.016

NOTES TO TABLE 2

1. The Δ, H + K, CNB, and MgG indices are those of Brodie and Hanes 1986; all the rest follow the Burstein *et al.* 1981 definitions.
2. Nomenclature for the Andromeda clusters follows Huchra, Stauffer, and van Speybroeck 1982, with the Battistini *et al.* 1980 number first followed by the Sargent *et al.* 1977 number. N188-Ave is the weighted average of the individual NGC 188 stars.
3. The errors are taken from Burstein *et al.* 1981 and Brodie and Hanes 1986 for the Galactic cluster indices, and are the photometric errors, σ_P, for our single or weighted averaged multiple observations of Andromeda clusters and Galactic stars. Where photon statistical errors were unavailable from the Brodie and Hanes, data, errors have been estimated based on the weighting factors they ascribed to their spectra.

instruments. There is a weak correlation for Hβ, but the error bars are large because of the difficulty in accurately measuring this narrow-band index, and the net offset is zero.

e) *Errors and Systematic Effects*

At resolutions of 5–12 Å, many of the weaker features contain little useful information. This statement also applies to the Na D feature, which, although it can be relatively strong, at low redshift lies underneath the strong low-pressure Na lamp lines produced by the cities of San Jose, Tucson, and Nogales. Other features, such as the DDO indices and Suntzeff's CA index, have large bandpasses and are defined over widely separated wavelength regions. The large bandpasses are advantageous because they allow indices to be measured with statistically higher accuracies, especially important in weak spectra. This advantage, however, is more than offset by the increased difficulty in obtaining good relative spectrophotometry over large-wavelength baselines in the presence of such effects as atmospheric dispersion, atmospheric extinction, S-distortion in the image tubes, and various flat-fielding inaccuracies.

Conversely, narrow-line indices are easy to measure even in flat-fielded but unrectified spectra, but are subject to large statistical uncertainties in poor signal-to-noise spectra. However, although an absolute continuum level is very difficult to define in late-type spectra, provided that care is taken to define continuum bandpasses that are free of strong features or blends, narrow-line indices should be stable and thus useful for comparative studies of objects from different populations. As we shall see below, this means that it may be possible to establish a relative metallicity scale based on narrow-band indices and colors.

In addition to measuring the statistical errors determined by photon statistics of individual measurements, we have also tried to estimate the systematic errors in our measurements by making repeated observations of several objects. This was facilitated by the fact that several objects in our sample have been used to define radial velocity templates for other programs employing the MMT spectrograph and were therefore observed repeatedly. Table 4 gives the measured dispersion of these multiple observations for the subset of indices we have elected to study. In general we find that our measurements of narrow-line indices are good to about 0.02 mag (or about 2%), which is just slightly worse than the error predicted by photon statistics.

The usefulness of a given index is determined by the ratio of its error to its range. We return to this point in § III*b*.

III. METALLICITY CALIBRATION

a) *The Calibration*

We have adopted the Zinn and West (1984) scale for Galactic globular cluster metallicities. This scale is based primarily

TABLE 3

COMPARISON WITH BFGK INDICES

Index	CNR	Hβ	MgH	Mg2	G Band	MgB
Mean difference	0.019	−0.001	−0.015	−0.017	0.010	0.004
Dispersion	0.030	0.025	0.021	0.031	0.029	0.021

NOTE.—Statistics for 34 objects in common (Andromeda clusters + Galactic stars).

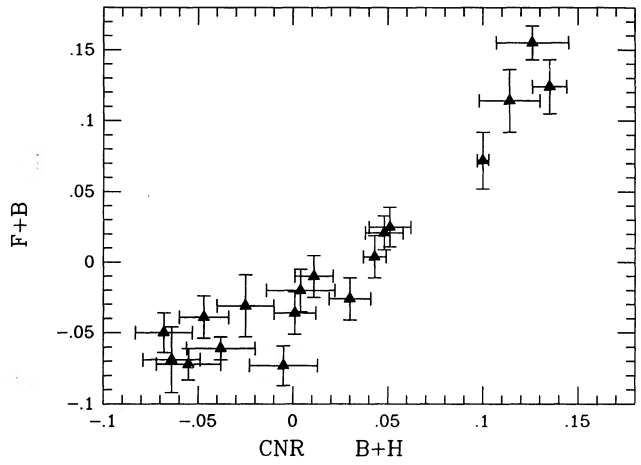

FIG. 2*a*

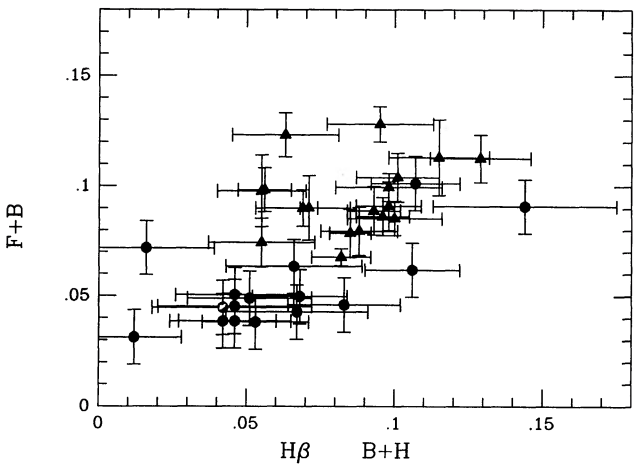

FIG. 2*b*

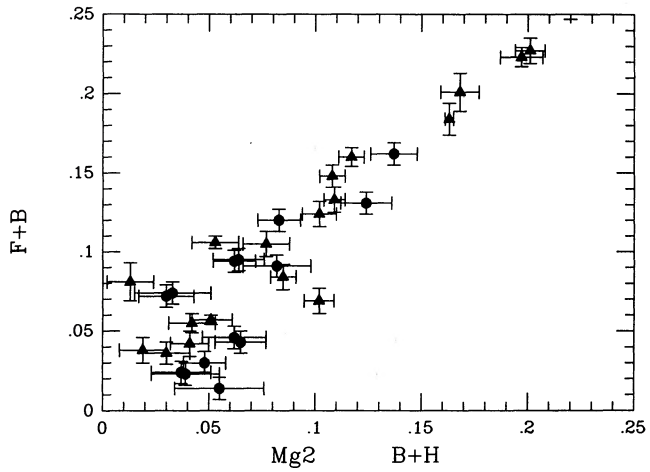

FIG. 2*c*

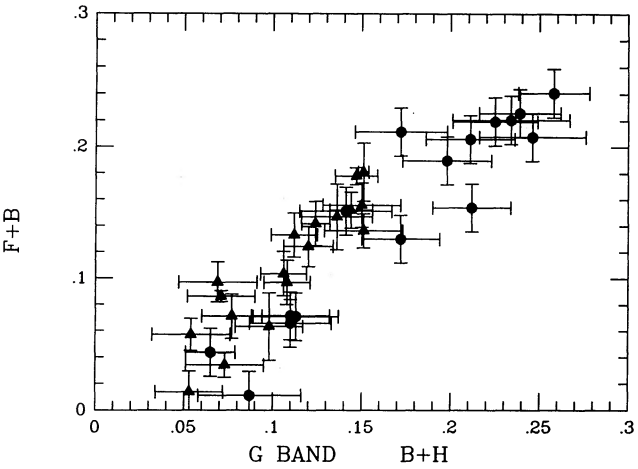

FIG. 2*d*

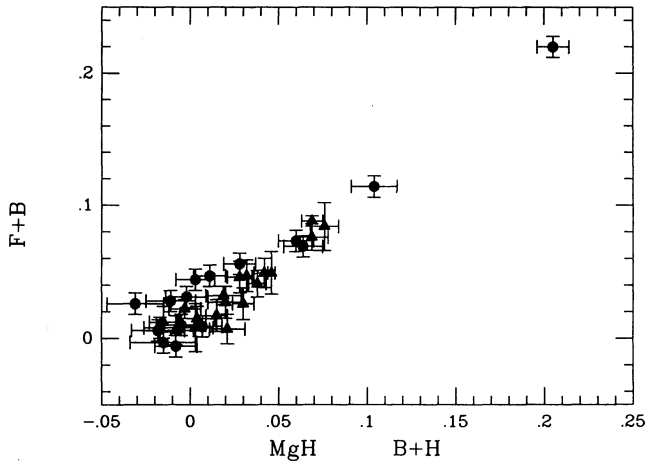

FIG. 2*e*

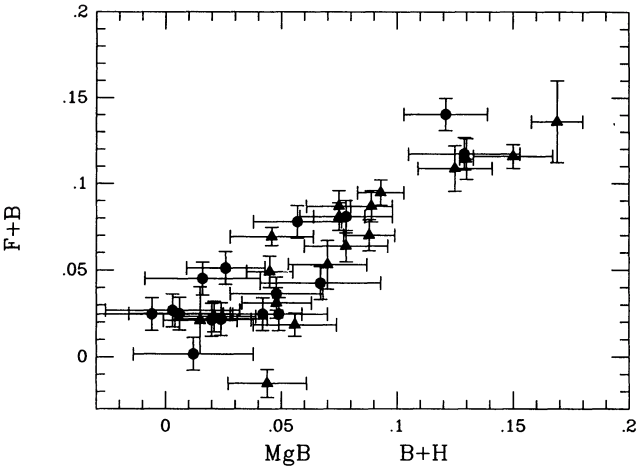

FIG. 2*f*

FIG. 2.—FBGK line indices (converted to our definition) plotted against our measurements for Andromeda globular clusters (*triangles*) and stars in Galactic globular clusters (*filled circles*). (*a*) CNR, (*b*) Hβ, (*c*) Mg2, (*d*) G band, (*e*) MgH, (*f*) MgB.

TABLE 4

DISPERSION OF MULTIPLE OBSERVATIONS

INDEX	225–280		NGC 4486B		ADOPTED
	σ	$\overline{\sigma_P}$	σ	$\overline{\sigma_P}$	σ_S
Δ	0.074	0.007	0.107	0.009	0.100
H+K	0.028	0.024	0.033	0.029	0.025
CNB	0.034	0.026	0.038	0.034	0.025
CNR	0.019	0.016	0.030	0.019	0.025
CH	0.024	0.021	0.025	0.025	0.015
Hβ	0.023	0.018	0.027	0.020	0.020
Mg2	0.028	0.012	0.025	0.014	0.025
MgH	0.019	0.011	0.021	0.012	0.020
Mgb	0.032	0.020	0.025	0.024	0.025
MgG	0.022	0.021	0.022	0.019	0.015
Fe52	0.034	0.017	0.025	0.019	0.025
Na I	0.040	0.023	0.037	0.027	0.030

NOTE.—σ is the dispersion of multiple measurements; $\overline{\sigma_P}$ is the average photon statistical error; and σ_S is the estimated instrumental error. There were 31 observations of N4486B and 27 of 225–280.

on a measure of the ultraviolet line blanketing in the integrated light of the globular clusters and has been checked against measurements and models of the spectra of individual stars in some of the clusters. While the absolute scale remains uncertain at the level of a few tenths dex in [Fe/H], the above calibration provides a convenient and robust ranking of the mean metal content of integrated stellar systems.

We have also used Zinn and West's Galactic globular cluster [Fe/H] values to derive a new calibration of the infrared colors ($V-K$, $J-K$, CO) versus metallicity (Aaronson *et al.* 1978; Frogel, Persson, and Cohen 1980, hereafter FPC). FPC derived these calibrations based on the old Zinn (1980*a*) metallicity scale. Cohen (1988) has kindly provided us with a table of the reddening-corrected infrared colors and estimated reddenings, $E(B-V)$, used by FPC. These colors have been reddening de-corrected and then recorrected using the new $E(B-V)$ estimates of Armandroff (1989). These colors were then plotted against the new metallicity estimates of Zinn and West (1984), and linear relationships fitted by two-sided linear regression. The raw infrared colors and the metallicities for our calibrators are given in Table 5.

Figure 3 shows the correlations between the IR colors and [Fe/H]. Our newly derived calibration relations are

$$[\mathrm{Fe/H}]_{V-K} = 1.574(V-K) - 5.110\,, \quad r = 0.83\,, \quad (10)$$

$$[\mathrm{Fe/H}]_{J-H} = 5.572(J-K) - 5.196\,, \quad r = 0.89\,, \quad (11)$$

$$[\mathrm{Fe/H}]_{\mathrm{CO}} = 17.730(\mathrm{CO}) - 2.096\,, \quad r = 0.86\,, \quad (12)$$

where r is the linear correlation coefficient. These relations reproduce the input [Fe/H] with dispersions of 0.27, 0.22, and 0.27, respectively.

We use the new calibration to derive metallicities for the Andromeda globular clusters with published infrared photometry (FPC; Bonoli *et al.* 1987). Table 6 lists the derived metallicities, [Fe/H], for these Andromeda globular clusters. These metallicities, and $[\mathrm{Fe/H}]_{V-K}$ in particular, are extremely sensitive to the assumed reddening. We have discarded from the calibration all clusters with $E(B-V) \geq 0.30$ and all clusters where the error on the mean value of the derived metallicity is greater than 0.2. Where an $[\mathrm{Fe/H}]_{\mathrm{CO}}$ estimate is not in agreement with $[\mathrm{Fe/H}]_{V-K}$ and $[\mathrm{Fe/H}]_{J-H}$, it has not been included in the final mean [Fe/H] adopted for that cluster.

Figure 4 shows the plots of a variety of our measured spectroscopic indices versus [Fe/H]. Table 7 gives the linear least-squares fits of index versus metallicity for the most metallicity-sensitive line indices derived from four subsamples:

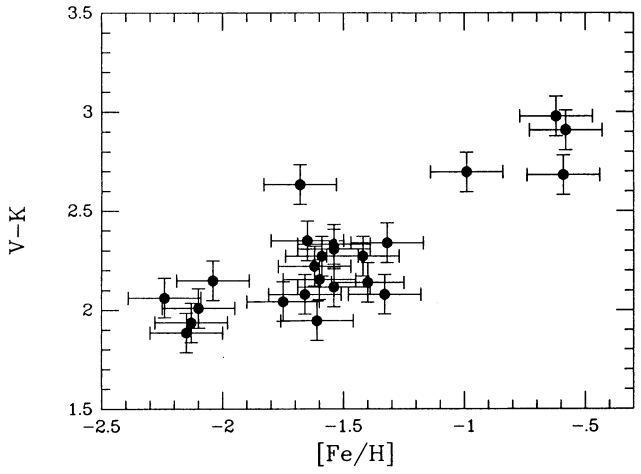

FIG. 3*a*

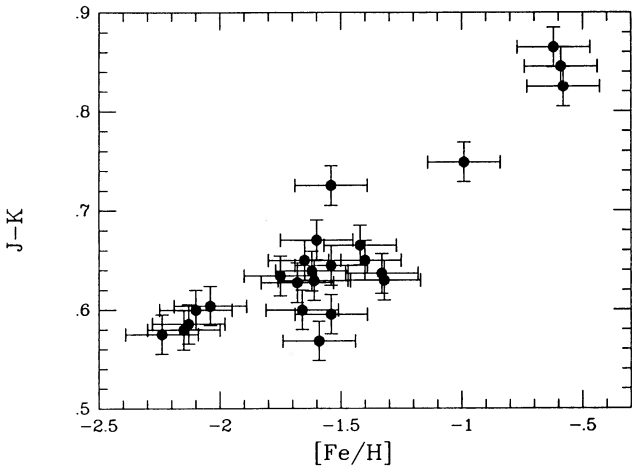

FIG. 3*b*

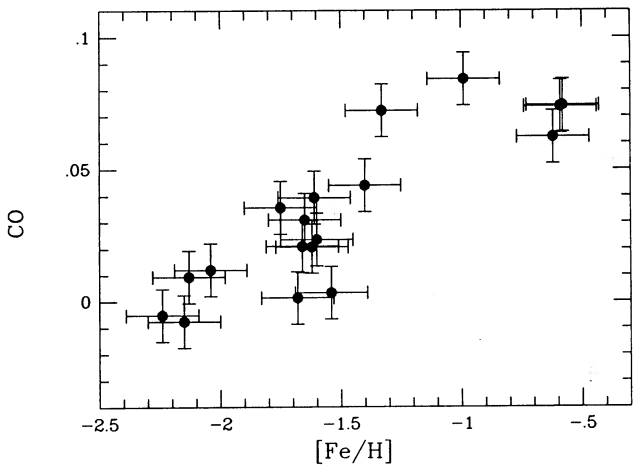

FIG. 3*c*

FIG. 3.—Infrared colors of Galactic globular clusters vs. [Fe/H]. (*a*) $V-K$, (*b*) $J-K$, (*c*) CO.

TABLE 5A

IR COLORS FOR CALIBRATING GALACTIC GLOBULARS

Name (NGC)	[Fe/H]	$U-B$	$B-V$	$V-K$	$J-H$	$H-K$	CO	H_2O	$E(B-V)$
5024.....	−2.04	0.04	0.58	2.01	0.48	0.10	0.02	0.06	0.00
5272.....	−1.66	0.07	0.66	2.08	0.53	0.07	0.02	0.02	0.01
5904.....	−1.40	0.07	0.63	2.14	0.57	0.08	0.04	0.01	0.03
6205.....	−1.65	0.00	0.62	2.35	0.57	0.08	0.03	0.03	0.02
6254.....	−1.60	0.08	0.67	2.21	0.58	0.10	0.02	0.04	0.28
6341.....	−2.24	−0.01	0.58	2.09	0.51	0.07	−0.01	0.02	0.02
6838.....	−0.58	0.46	0.95	2.88	0.69	0.13	0.08	0.05	0.27
7006.....	−1.59	0.07	0.66	2.05	0.47	0.06	...	...	0.05
7078.....	−2.15	−0.02	0.58	1.83	0.48	0.09	−0.01	0.02	0.10
7089.....	−1.62	0.02	0.59	2.11	0.54	0.08	0.02	0.03	0.02
7099.....	−2.13	0.01	0.55	2.02	0.50	0.10	0.01	0.04	0.04
1904.....	−1.69	−0.04	0.55	...	0.51	0.07	...	...	0.01
2419.....	−2.10	0.05	0.65	2.01	0.57	0.03	...	...	0.03
5634.....	−1.82	0.04	0.58	...	0.50	0.08	0.05	0.05	0.04
6093.....	−1.68	0.05	0.64	2.30	0.50	0.07	0.01	0.04	0.16
6218.....	−1.61	0.04	0.61	1.89	0.53	0.09	0.04	0.09	0.17
6229.....	−1.54	0.09	0.69	2.28	0.56	0.08	...	...	0.00
6356.....	−0.62	0.40	0.89	2.95	0.69	0.17	0.06	0.05	0.27
6637.....	−0.59	0.12	0.83	2.71	0.71	0.14	0.07	0.06	0.18
6715.....	−1.42	0.14	0.67	2.30	0.57	0.10	...	...	0.15
6864.....	−1.32	0.14	0.65	2.34	0.55	0.08	...	...	0.17
6934.....	−1.54	0.12	0.67	2.20	0.52	0.09	...	0.03	0.15
6981.....	−1.54	0.15	0.70	2.36	0.61	0.12	...	...	0.04

TABLE 5B

IR COLORS FOR NONCALIBRATING GALACTIC GLOBULARS

Name (NGC)	[Fe/H]	$U-B$	$B-V$	$V-K$	$J-H$	$H-K$	CO	H_2O	$E(B-V)$
High Reddening									
6273.....	−1.68	0.03	0.55	1.98	0.53	0.07	0.02	0.02	0.36
6284.....	−1.40	0.12	0.62	2.13	0.58	0.07	...	...	0.29
6293.....	−1.92	−0.01	0.55	1.87	0.49	0.04	...	...	0.37
6333.....	−1.78	−0.02	0.54	2.06	0.53	0.07	0.04	0.05	0.34
6402.....	−1.39	0.18	0.68	2.17	0.59	0.09	0.05	0.06	0.59
6440.....	−0.26	0.44	0.83	2.62	0.70	0.12	0.10	0.05	1.10
6544.....	−1.56	0.07	0.58	2.03	0.59	0.06	0.04	0.01	0.79
6626.....	−1.44	0.12	0.64	2.17	0.58	0.08	0.06	0.05	0.40
6638.....	−1.15	0.23	0.73	2.59	0.64	0.09	...	...	0.41
6712.....	−1.01	0.26	0.78	2.60	0.66	0.16	0.09	0.06	0.48
6779.....	−1.94	0.03	0.61	2.09	0.51	0.11	0.03	0.04	0.21
Poorly Determined Reddening									
288.....	−1.40	0.09	0.65	...	0.59	0.13	...	...	0.04
6517.....	−1.34	0.04	0.65	...	0.50	0.05	0.05	0.04	1.08
6535.....	−1.75	0.04	0.58	...	0.78	0.05	...	...	0.32
6539.....	−0.66	0.13	0.67	2.19	0.65	0.07	0.13	0.08	0.91
6760.....	−0.52	0.25	0.73	2.40	0.67	0.12	0.10	0.10	0.71
6121.....	−1.33	0.09	0.45	2.33	0.60	0.08	0.06	0.01	0.40
6171.....	−0.99	0.21	0.69	2.53	0.61	0.11	0.09	0.05	0.31
6656.....	−1.75	−0.04	0.57	1.96	0.56	0.06	0.04	0.04	0.32

(1) the calibrating Galactic globular clusters, (2) the calibrating Galactic clusters augmented with individual red giant stars in NGC 188, (3) the Andromeda clusters with [Fe/H] from IR colors, and (4) the combined sample of Galactic and Andromeda clusters and NGC 188. Because it is desirable to extend our calibration to solar metallicity and above, we have measured several individual giant stars in the open cluster NGC 188: I-1, I-57, II-51, II-72, II-76, and II-88. NGC 188 is an old open cluster which is generally agreed to have approximately solar abundance (Sandage 1962; Janes 1979). For those indices where the NGC 188 stars appear to lie on a simple extrapolation of the globular cluster relationship, we have computed a regression through the augmented sample (sample 4 above). Table 7 lists the values of the slope a and intercept b, and their errors; the linear correlation coefficient; $\sigma_{[Fe/H]}$, the sigma of the fit in [Fe/H], defined by

$$\sigma^2_{[Fe/H]} = \frac{\sum ([Fe/H]_p - [Fe/H]_o)^2}{N-1}, \quad (13)$$

where $[Fe/H]_p$ is the metallicity predicted by the simple linear relation

$$[Fe/H] = aI + b\ ; \quad (14)$$

TABLE 6

M31 CLUSTER [Fe/H]'S FROM IR COLORS

Name (1)	$[Fe/H]_{V-K}$ (2)	$[Fe/H]_{J-K}$ (3)	$[Fe/H]_{CO}$ (4)	$[Fe/H]_{IR} \pm \sigma$ (5)
000–1	−1.36	−1.01	−1.03	−1.19 ± 0.25
000–33	−1.87	−1.83	...	−1.85 ± 0.03
006–58	−0.80	−1.06	...	−0.93 ± 0.19
012–64	−2.06	−2.19	...	−2.12 ± 0.10
019–72	−1.13	−1.08	...	−1.10 ± 0.03
020–73	−1.18	−1.34	...	−1.26 ± 0.12
000–76	−1.40	−1.34	−1.65	−1.37 ± 0.04
058–119	−1.41	−1.51	...	−1.46 ± 0.07
000–127	−1.41	−1.40	...	−1.40 ± 0.01
158–213	−1.10	−1.01	−0.06	−1.05 ± 0.06
163–217	−0.51	−0.37	−0.15	−0.44 ± 0.10
000–219	−2.17	−1.79	...	−1.98 ± 0.27
171–222	−0.64	−0.56	...	−0.60 ± 0.06
179–230	−1.62	−1.06	...	−1.34 ± 0.39
182–233	−1.43	−1.23	...	−1.33 ± 0.14
193–244	−0.53	−0.56	...	−0.55 ± 0.02
205–256	−1.16	−1.12	...	−1.14 ± 0.03
212–263	−1.71	−1.62	...	−1.67 ± 0.06
218–272	−1.08	−0.90	−0.77	−0.99 ± 0.13
224–279	−2.02	−2.01	...	−2.02 ± 0.01
225–280	−0.64	−0.56	−0.23	−0.60 ± 0.06
240–302	−1.87	−1.51	...	−1.69 ± 0.25
M31 nucleus	0.04	0.00	0.74	0.02 ± 0.03

NOTE.—"Errors" in col. (5) are only the dispersion of the two estimates from $V-K$ and $J-K$.

and the dispersion of the index about the regression line,

$$\sigma_M^2 = \frac{\sum (I_p - I_o)^2}{N-1}, \quad (15)$$

where I_p is the value of the index predicted by the inverse of equation (13). The dispersion σ_M is valuable in assessing the ability of a given index to measure mean metallicity; we will use this later in an estimate of the error associated with each measurement.

For several indices, there is only a weak correlation with metallicity, e.g., Hβ, which is weakly anticorrelated with [Fe/H]. For several other indices there are indications that fitting the entire region between $-2.0 < [Fe/H] < 0.0$ with a single straight line may be an oversimplification. A good example of this is the H+K index, which, although linear at low metallicities, "saturates" or flattens out above [Fe/H] ~ -1. Another example is the Δ index, which has a very high correlation coefficient and small scatter, but which might be slightly better fitted by a second-order polynomial.

Six features correlate extremely well with [Fe/H], as indicated by their large correlation coefficients. The criterion for the inclusion of a particular index in the derivation of [Fe/H] is that the full range of values of the index be large compared with the scatter in the index versus [Fe/H] relation. If the correlation coefficient is ≥ 0.80, this criterion is probably satisfied. This is true for Δ, Mg2, MgH, CH (the G band), CNB, and FE52. The correlation coefficients for Mgb and MgG are also 0.80 or above, but, since Mgb, MgG, and Mg2 measure essentially the same feature, the best of the three, Mg2, was adopted for our calibration.

Although we have included the Andromeda clusters with metallicities from IR colors as calibrating objects, the plots of index versus metallicity reveal a slight offset in CNB between the Galactic clusters and the Andromeda clusters in the sense that the Andromeda cluster line strengths are enhanced with respect to the Galactic clusters. A similar offset is seen in H+K, and a much more striking offset is apparent in CNR. However, the relatively low correlation coefficients for CNR and H+K have, in any case, precluded their use as metallicity indicators. For other indices (e.g., Δ, CH, and MgH) there is little or no offset, and the Galactic and Andromeda clusters follow nearly the same relation.

We considered three possible explanations for the offsets. First, the infrared colors and/or the reddenings for the M31 clusters may be systematically in error. While such errors may exist, it is difficult to account for the fact that they do not produce offsets for all indices. Neither the size nor the locations of the CNR bandpasses would cause it to be particularly sensitive to reddening errors. Second, the Galactic globular cluster indices and the Andromeda cluster indices may be on different scales because of instrumental effects. The Galactic globular measurements were made at Lick and at the AAT using the ITS and the IPCS, respectively. The Andromeda indices were measured at the MMT using a photon-counting Reticon system. These spectrograph and detector systems have different characteristics, most importantly with respect to scattered light. Again, a scattered-light problem would have to affect one index and not the others. Plots of our indices against those of BFGK (Fig. 2) show excellent agreement, which argues against a scattered-light problem. The Brodie and Hanes (1986) measurements were made, for the most part, with the same ITS instrument. In fact, if the MMT data are corrected for scattered light/light-induced background (about a 3% effect; J. Biretta 1987, private communication) the offset is *increased* rather than decreased. Last, the Andromeda globulars may exhibit abundance anomalies with respect to the Galactic globulars. BFGK report anomalously strong CNR and Hβ in Andromeda globulars compared with Galactic globulars, and Tripicco (1989) has found strong CN in metal-rich Andromeda globu-

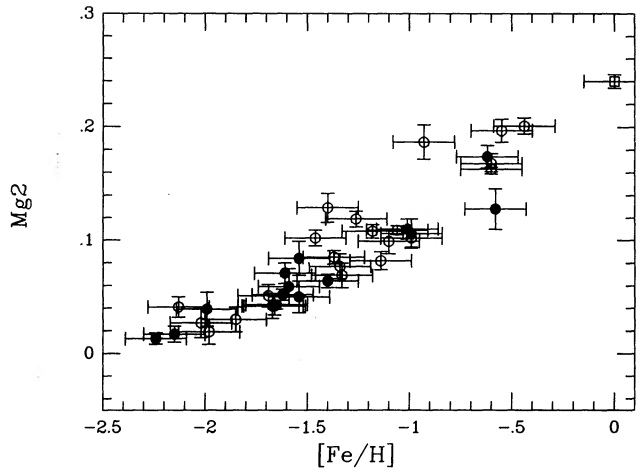

FIG. 4a

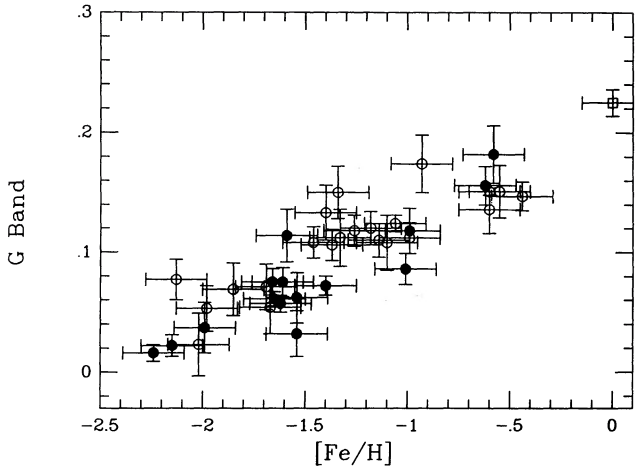

FIG. 4b

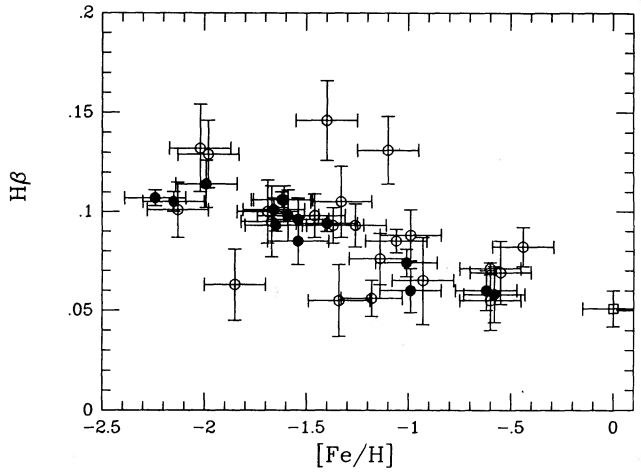

FIG. 4c

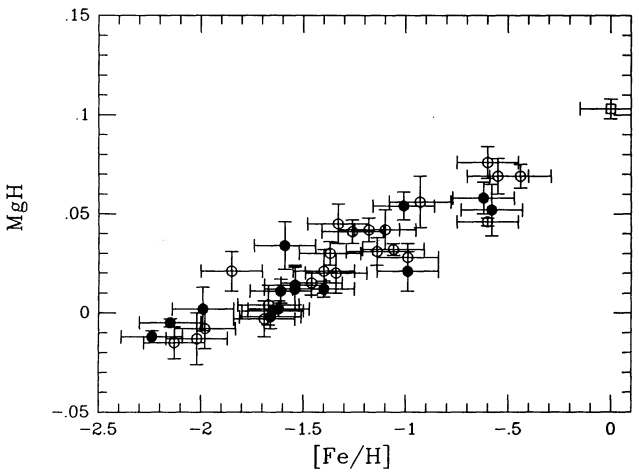

FIG. 4d

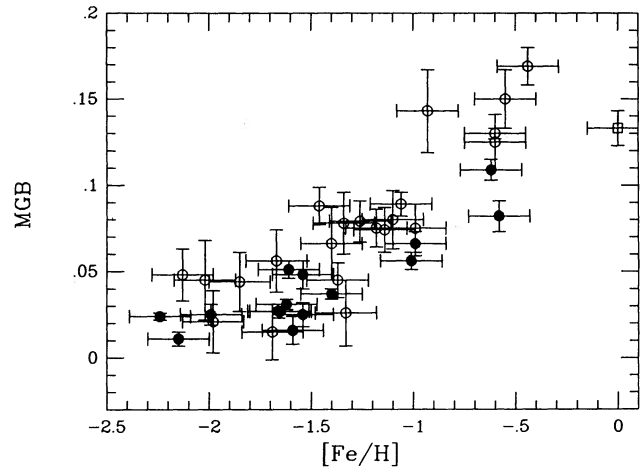

FIG. 4e

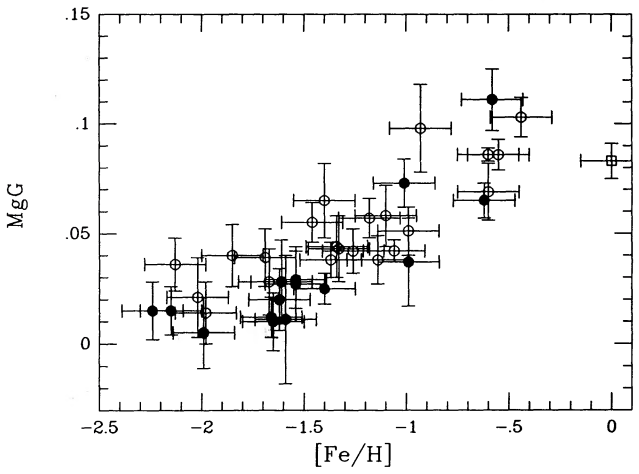

FIG. 4f

FIG. 4.—(*a*) Index vs. metallicity, [Fe/H], for Galactic globular clusters (*filled circles*), Andromeda globular clusters (*open circles*), and the mean of six NGC 188 giants (*square*). For the Andromeda globular clusters, [Fe/H] has been estimated from infared colors alone. (*a*) Mg2, (*b*) G band, (*c*) Hβ, (*d*) MgH, (*e*) Mgb, (*f*) MgG, (*g*) Δ, (*h*) H + K, (*i*) CNB, (*j*) CNR, (*k*) Fe 5270 Å, (*l*) Na I.

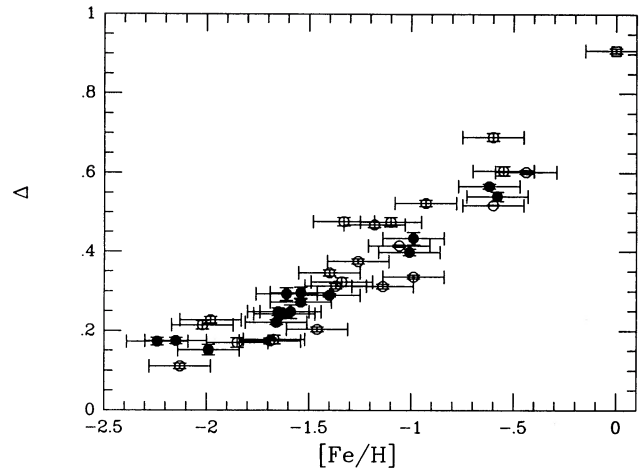

FIG. 4*g*

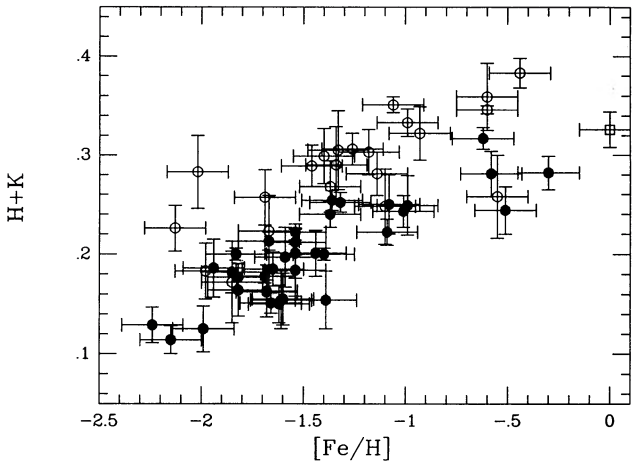

FIG. 4*h*

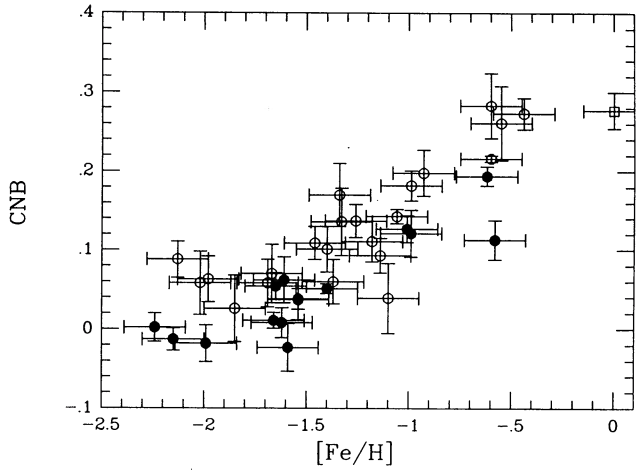

FIG. 4*i*

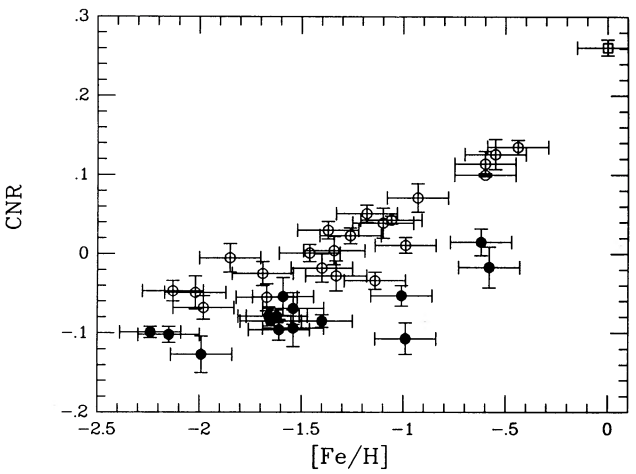

FIG. 4*j*

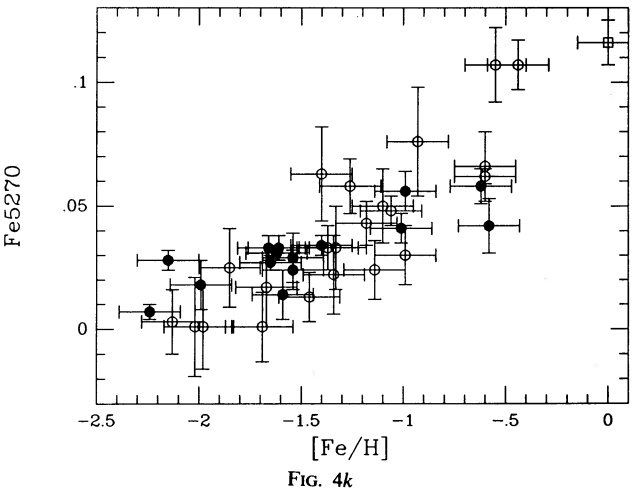

FIG. 4*k*

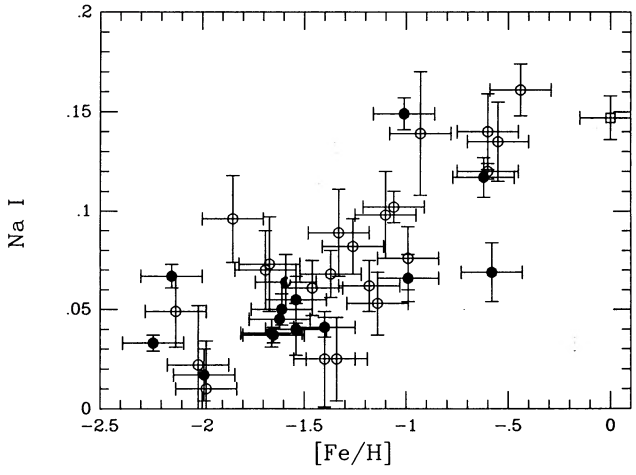

FIG. 4*l*

TABLE 7

REGRESSIONS OF INDEX AND [Fe/H]

Index	Sample	r	a	b	$\sigma_{Fe/H}$	σ_M
CH (G band)	GG	0.93	11.11	−2.33	0.22	0.020
	GG+188	0.95	10.78	−2.31	0.22	0.020
	AND	0.83	13.00	−2.70	0.28	0.021
	All	0.89	11.42	−2.46	0.26	0.023
Hβ	GG	−0.90	−28.92	1.17	0.26	0.009
	GG+188	−0.92	−30.33	1.30	0.27	0.009
	AND	−0.49	−23.16	0.82	0.55	0.024
	All	−0.67	−25.03	0.93	0.47	0.019
Mg2	GG	0.95	12.67	−2.34	0.18	0.014
	GG+188	0.95	11.13	−2.25	0.21	0.019
	AND	0.92	8.74	−2.15	0.20	0.022
	All	0.92	9.92	−2.21	0.22	0.023
MgH	GG	0.90	25.77	−1.88	0.27	0.010
	GG+188	0.91	22.30	−1.83	0.28	0.012
	AND	0.92	18.66	−1.83	0.19	0.010
	All	0.91	20.58	−1.84	0.24	0.012
Mgb	GG	0.91	20.71	−2.33	0.25	0.012
	GG+188	0.93	19.17	−2.27	0.25	0.013
	AND	0.86	11.60	−2.19	0.26	0.022
	All	0.81	14.17	−2.22	0.35	0.024
MgG	GG	0.82	16.96	−2.03	0.27	0.016
	GG+188	0.83	18.42	−2.06	0.29	0.016
	AND	0.83	20.81	−2.37	0.28	0.014
	All	0.82	18.41	−2.13	0.30	0.016
Δ	GG	0.96	3.87	−2.61	0.13	0.033
	GG+188	0.95	3.31	−2.46	0.16	0.049
	AND	0.90	3.00	−2.38	0.21	0.069
	All	0.93	3.18	−2.43	0.18	0.057
H+K	GG	0.84	9.52	−3.37	0.25	0.026
	GG+188	0.87	9.87	−3.43	0.25	0.026
	AND	0.74	9.33	−3.94	0.35	0.037
	All	0.73	7.93	−3.23	0.37	0.047
CNB	GG	0.86	8.36	−1.92	0.23	0.028
	GG+188	0.90	7.82	−1.90	0.23	0.029
	AND	0.83	6.40	−2.11	0.33	0.043
	All	0.83	6.57	−1.94	0.29	0.044
CNR	GG	0.85	14.00	−0.42	0.32	0.024
	GG+188	0.78	7.82	−0.90	0.44	0.056
	AND	0.90	8.07	−1.43	0.22	0.027
	All	0.75	7.34	−1.19	0.41	0.056
FE52	GG	0.90	37.00	−2.65	0.27	0.007
	GG+188	0.87	27.09	−2.34	0.33	0.012
	AND	0.86	15.65	−1.91	0.25	0.016
	All	0.83	20.37	−2.09	0.33	0.016
Na I	GG	0.73	17.75	−2.50	0.44	0.025
	GG+188	0.79	17.24	−2.47	0.42	0.025
	AND	0.77	12.04	−2.24	0.33	0.027
	All	0.76	14.46	−2.36	0.39	0.027

NOTE.—GG = Galactic globulars (36 objects for the BH indices, 17 objects for the FB indices); GG+188 = GG+NGC 188 giant average (37 objects for the BH indices, 18 objects for the FB indices); AND = Andromeda clusters with [Fe/H] from IR colors (22 objects); All = all 59 objects for the BH indices, 40 for the FB indices.

lars. There is no convincing offset for Hβ in our data. We note that BFGK plot their indices against Mg2 and not [Fe/H]. In Figure 5 we plot CNR, CNB, H+K, and Hβ against Mg2 for all the Andromeda clusters with high signal-to-noise spectra, not just those for which an [Fe/H] estimate exists. There is still no offset for Hβ, although three or four clusters appear to have unusually strong Hβ, perhaps indicating a young stellar population. The offset in CNB has mostly disappeared. The offsets in CNR and H+K are still quite pronounced.

An abundance anomaly appears to be the most likely explanation for the observed offsets. Both the CNB and the CNR bandpasses contain metallic-line contributions from elements other than cyanogen. In some cases, these other elements may dominate the response of the index to changes in [Fe/H]. A stronger contribution to CNB from other metallic lines (e.g., Mg and Fe) may explain the smaller offset in CNB compared with CNR. A contribution to both CNB and CNR from other metallic lines may explain the fact that both indices exhibit an

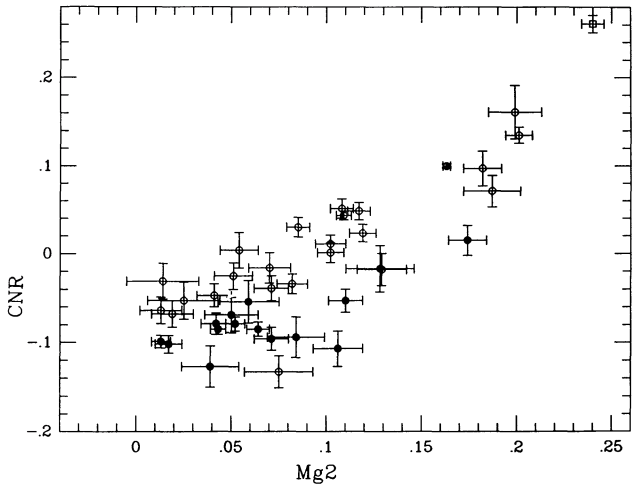

FIG. 5a

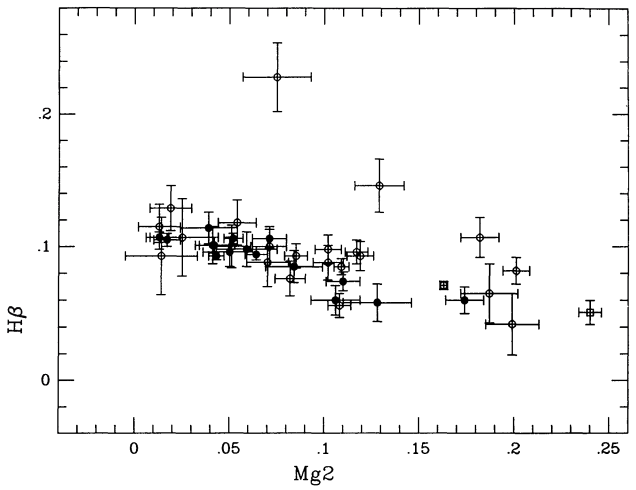

FIG. 5b

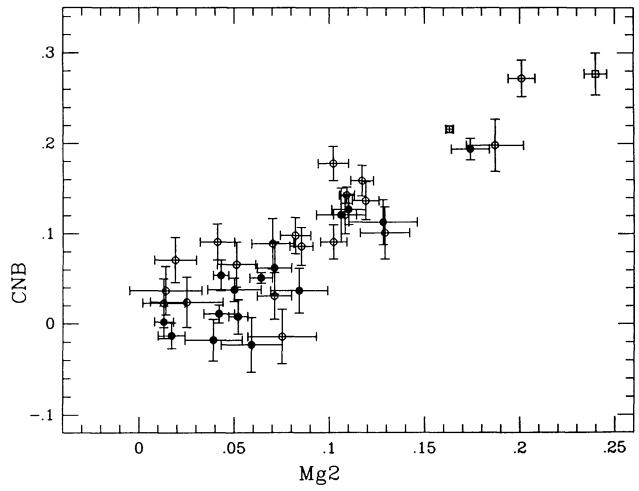

FIG. 5c

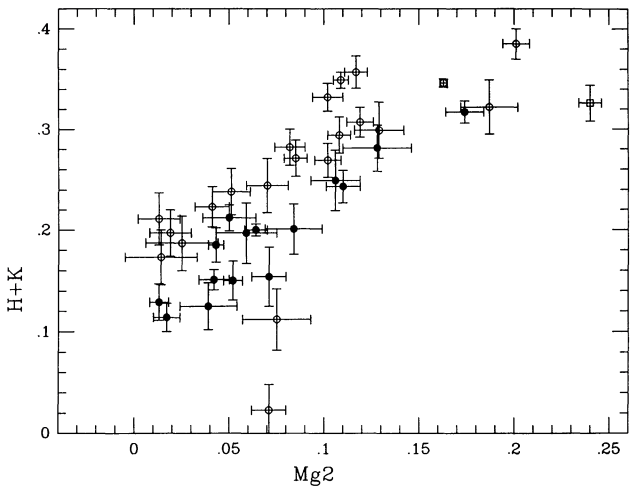

FIG. 5d

FIG. 5.—(*a*) CNR vs. Mg2. (*b*) Hβ vs. Mg2. (*c*) CNB vs. Mg2. (*d*) H + K vs. Mg2. Symbols as in Fig. 4.

offset at the lowest [Fe/H] values, where cyanogen should be virtually undetectable (Smith 1987). If the cyanogen enhancement is due to an overabundance of nitrogen, then a deepening of the cores of Ca II H and K lines with respect to the wings is to be expected, at least in red giants (Norris 1978). A direct measurement of NH at 3360 Å would be useful in establishing nitrogen as the culprit of the abundance anomaly. A more detailed discussion of abundance anomalies and the relationship between line strengths in globular clusters and line strengths in galaxies will follow in a subsequent paper.

Although the offset in CNB is of concern, we have decided to include CNB as a predictor of mean metallicity because of its strong correlation with [Fe/H] for the calibrators and because CN is a contributor to [Fe/H]. The lack of an offset for the high signal-to-noise data in the CNB–Mg2 plane lends further support to this selection. Because of the weighting scheme employed (see below), the inclusion of CNB as a metallicity estimator changes the final [Fe/H] estimate for a cluster by, at most, 0.1 dex and by 0.02 dex on average.

b) Techniques

There are several possible schemes for deriving an estimate of the mean [Fe/H] for an object from several indices. Perhaps the best known is the simple average, where each index is assumed to provide an estimate of equal weight. In this case the estimate of [Fe/H] is just

$$[\mathrm{Fe/H}]_A = \frac{\sum [\mathrm{Fe/H}]_I}{N}, \tag{16}$$

and the estimate of the error in the mean is just

$$\sigma_A^2 = \frac{\sum ([\mathrm{Fe/H}]_I - [\mathrm{Fe/H}]_A)^2}{N(N-1)}. \tag{17}$$

It is also possible to derive a weighted average based on the errors associated with the [Fe/H] estimate from each individual index. In particular, the form of such an estimate would be

$$[\mathrm{Fe/H}]_W = \frac{\sum (W_I[\mathrm{Fe/H}]_I)}{\sum W_I}, \tag{18}$$

where the weights, W_I, could be derived from the scaled inverse of an error estimator, σ_I, one example of which is the quadrature sum

$$\sigma_I = (\sigma_M^2 + \sigma_S^2 + \sigma_P^2)^{1/2}; \tag{19}$$

σ_M is the "index error" discussed above, defined in equation (14) and given in Table 7, σ_P is the photon statistical error defined in equation (6), and σ_S is the error associated with our ability to measure the same index repeatedly (see Table 4 and HBS). As σ_I is in similar "units" for all indices (magnitudes), but since we want to compare the relative merits of different indices with very different ranges as well as different sensitivities to [Fe/H], we construct our weights as

$$W_I = \frac{R_I}{\sigma_I}, \tag{20}$$

where R_I is the "range" spanned by an index for a change of 1.0 in [Fe/H]. Such a definition will give high weight to an index with large range and small dispersion and which is easily measured. It also allows for the inclusion of measurement errors and leads to a natural figure of merit for each index,

$$G(I) = \frac{R_I}{(\sigma_S^2 + \sigma_M^2)^{1/2}}. \tag{21}$$

With these estimates for the weights of the individual [Fe/H] estimates, the error in the combined [Fe/H] estimate is then

$$\sigma_W = [\sum W_I]^{-1/2}[\sum W_I([\mathrm{Fe/H}]_I - [\mathrm{Fe/H}]_W)^2]^{1/2}. \tag{22}$$

A third useful possibility is to take the median of the estimates of [Fe/H]. The median is a statistic well known for its insensitivity to outliers (Hoaglin, Mosteller, and Tukey 1983), which is a property that is especially important in the presence of low signal-to-noise data, possible systematic problems with spectrophotometry, or abundance anomalies. For this estimator, the usual estimate of the error is the median absolute deviation from the median, MAD, defined by

$$\mathrm{MAD} = \mathrm{MED}([\mathrm{Fe/H}]_I - [\mathrm{Fe/H}]_M). \tag{23}$$

IV. RESULTS

In order to check our calibration and to determine which of the possible techniques discussed above yields the most efficient and/or minimum-bias estimate of the metallicity, we have worked backward and applied our calibrations to the index measurements of the calibrating clusters.

Table 8 and Figure 6 show the results of this exercise. Listed in the table are the final mean, weighted mean, and median estimated values of [Fe/H] and their associated errors for all our calibrating objects. The median absolute deviation from the median for a normal distribution is smaller than the "sigma" by a factor of 1/0.667, so we have scaled the MAD upward by that amount (Li 1985). The first column of the table

TABLE 8

CLOSING THE LOOP

Name (1)	[Fe/H] (2)	Average (3)	Weighted Average (4)	Median (5)
000–001	−1.18	−1.09 ± 0.14	−1.09 ± 0.13	−1.11 ± 0.14
000–33	−1.85	−1.70 ± 0.18	−1.74 ± 0.16	−1.72 ± 0.23
6–58	−0.93	−0.58 ± 0.13	−0.57 ± 0.12	−0.59 ± 0.16
12–64	−2.13	−1.85 ± 0.34	−1.81 ± 0.29	−1.94 ± 0.31
19–72	−1.10	−1.18 ± 0.25	−1.19 ± 0.22	−1.14 ± 0.19
20–73	−1.26	−1.05 ± 0.12	−1.07 ± 0.11	−1.04 ± 0.08
000–76	−1.37	−1.37 ± 0.17	−1.37 ± 0.15	−1.39 ± 0.14
58–119	−1.46	−1.46 ± 0.31	−1.42 ± 0.25	−1.38 ± 0.25
000–127	−1.40	−1.11 ± 0.22	−1.13 ± 0.20	−1.11 ± 0.39
158–213	−1.06	−1.10 ± 0.30	−1.09 ± 0.26	−1.11 ± 0.07
163–217	−0.44	−0.33 ± 0.23	−0.37 ± 0.23	−0.32 ± 0.27
000–219	−1.98	−1.87 ± 0.18	−1.84 ± 0.17	−1.93 ± 0.20
171–222	−0.60	−0.46 ± 0.28	−0.45 ± 0.26	−0.41 ± 0.38
179–230	−1.34	−1.25 ± 0.35	−1.22 ± 0.31	−1.41 ± 0.19
182–233	-1.33	−1.17 ± 0.26	−1.16 ± 0.24	−1.11 ± 0.29
193–244	−0.55	−0.34 ± 0.42	−0.38 ± 0.34	−0.34 ± 0.21
205–256	−1.14	−1.36 ± 0.19	−1.34 ± 0.16	−1.36 ± 0.17
212–263	−1.67	−1.75 ± 0.18	−1.75 ± 0.16	−1.78 ± 0.07
218–272	−0.99	−1.20 ± 0.35	−1.17 ± 0.30	−1.23 ± 0.14
224–279	−2.02	−1.94 ± 0.48	−1.91 ± 0.41	−2.00 ± 0.22
225–280	−0.60	−0.72 ± 0.17	−0.70 ± 0.15	−0.76 ± 0.14
240–302	−1.69	−1.80 ± 0.31	−1.76 ± 0.25	−1.79 ± 0.19
NGC 188–Ave	0.00	0.20 ± 0.40	0.18 ± 0.35	0.22 ± 0.12
NGC 5024	−1.99	−1.90 ± 0.19	−1.92 ± 0.16	−1.88 ± 0.17
NGC 5272	−1.66	−1.71 ± 0.18	−1.74 ± 0.16	−1.76 ± 0.17
NGC 5904	−1.40	−1.55 ± 0.06	−1.57 ± 0.05	−1.59 ± 0.05
NGC 6171	−0.99	−1.14 ± 0.13	−1.14 ± 0.11	−1.13 ± 0.08
NGC 6205	−1.65	−1.69 ± 0.10	−1.70 ± 0.08	−1.70 ± 0.15
NGC 6218	−1.61	−1.53 ± 0.22	−1.54 ± 0.18	−1.52 ± 0.08
NGC 6229	−1.54	−1.57 ± 0.13	−1.57 ± 0.13	−1.54 ± 0.16
NGC 6341	−2.24	−2.03 ± 0.14	−2.04 ± 0.13	−2.01 ± 0.12
NGC 6356	−0.62	−0.67 ± 0.08	−0.64 ± 0.08	−0.66 ± 0.03
NGC 6712	−1.01	−1.14 ± 0.25	−1.15 ± 0.22	−1.14 ± 0.11
NGC 6838	−0.58	−0.87 ± 0.28	−0.85 ± 0.26	−0.86 ± 0.36
NGC 6981	−1.54	−1.70 ± 0.20	−1.72 ± 0.19	−1.64 ± 0.12
NGC 7006	−1.59	−1.58 ± 0.36	−1.58 ± 0.33	−1.63 ± 0.46
NGC 7078	−2.15	−1.93 ± 0.22	−1.98 ± 0.17	−1.98 ± 0.13
NGC 7089	−1.62	−1.72 ± 0.17	−1.74 ± 0.14	−1.75 ± 0.11

NOTE.—Error in median is the median absolute deviation (MAD).

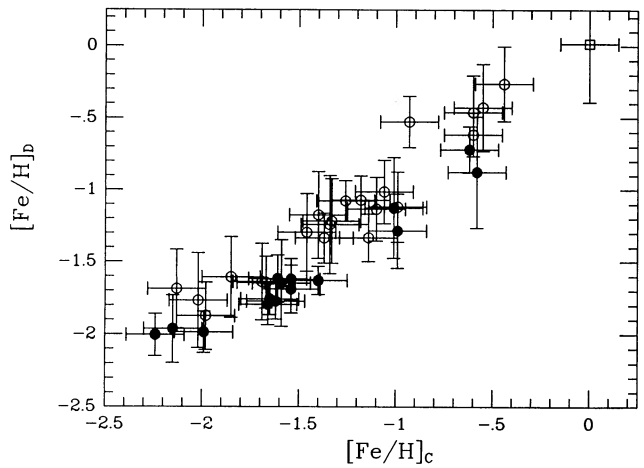

FIG. 6.—Metallicities derived from line-strength indices, $[Fe/H]_D$, vs. input calibrating metallicities. The derived metallicities are the weighted means of estimates from the index-metallicity equations in Table 9.

TABLE 9

CALIBRATION RELATIONS

Relation	Range	$G(I)$
Primary Calibrators		
$[Fe/H]_{\Delta} = 3.179 \times (\Delta) - 2.428$	0.315	2.74
$[Fe/H]_{Mg2} = 9.921 \times (Mg2) - 2.212$	0.101	2.97
$[Fe/H]_{MgH} = 20.578 \times (MgH) - 1.840$	0.049	2.10
$[Fe/H]_{G} = 11.415 \times (CH) - 2.455$	0.088	3.21
$[Fe/H]_{CNB} = 6.574 \times (CNB) - 1.940$	0.152	3.00
$[Fe/H]_{Fe52} = 20.367 \times (HK) - 2.086$	0.049	1.65
Poorer Calibrators		
$[Fe/H]_{CNR} = 7.344 \times (CNR) - 1.192$	0.136	2.22
$[Fe/H]_{H+K} = 7.929 \times (HK) - 3.225$	0.126	2.37
$[Fe/H]_{Na\ I} = 14.459 \times (Na\ I) - 2.360$	0.069	1.71
Redundant Indices		
$[Fe/H]_{MgB} = 14.171 \times (MgB) - 2.216$	0.071	2.05
$[Fe/H]_{MgG} = 18.407 \times (MgG) - 2.129$	0.054	2.46

gives the object name, while the second column gives the input value of [Fe/H].

As mentioned in § IIIa, for M31 clusters the values of [Fe/H] derived from the infrared colors, i.e., the input metallicities used in deriving the index-metallicity relations, depend very sensitively on the assumed reddening. If the reddening correction is in error for a particular cluster, the metallicity derived from the line indices will differ from the metallicity derived from the IR color. This suggests a method of establishing reddenings for M31 clusters. Such a method should provide $E(B-V)$ estimates good to about 0.04, since the line index metallicities are good to about 0.15 dex and the dispersion in the $V-K$ versus [Fe/H] relation is about 0.08. A knowledge of the reddening to this level of accuracy is important in a variety of contexts. For example, the Andromeda globular cluster luminosity function is critical in the use of clusters as extragalactic distance indicators and in estimations of H_0 based on the distance to the Virgo Cluster (e.g., Harris 1988).

The minimum-bias estimator is usually taken to be that estimator which yields the minimum mean deviation from the input values. All three of our estimators show essentially no mean deviation (two by construction).

The most efficient estimator is usually taken to be that estimator with the smallest variance defined as

$$\text{Variance} = \sigma^2 = \frac{\sum ([Fe/H]_{\text{estimated}} - [Fe/H]_{\text{input}})^2}{N-1} . \quad (24)$$

Again, all three or our estimators are similar; however, the weighted mean is slightly preferred with a variance of 0.0232 compared to 0.0238 for the unweighted mean and 0.0253 for the median. Any of the three can be used to derive estimates for [Fe/H] with an error of about 15%.

V. SUMMARY

Six spectral features in the integrated spectra of old stellar populations are found to correlate strongly with mean metal abundance, [Fe/H]. We propose that these indices can be used to estimate metallicities for integrated old stellar systems. The calibrating equations that we have chosen to adopt for these indices are given in Table 9, along with the index range and the figure of merit, $G(I)$, derived from equation (20).

We have found that the weighted mean of these individual estimates is the minimum-bias estimator, and we believe that one should quote its associated error. We therefore recommend that the first six equations in Table 9 be used to estimate metallicity and that the uncertainty in the weighted mean [Fe/H] be derived from equation (21).

This work has been supported by the Smithsonian Institution and by faculty research funds granted by the University of California, Santa Cruz. We would like to thank the telescope operators at the MMT, John McAffee, Janet Robertson, and Carol Heller, for putting up with large numbers of settings. We would also like to thank S. Tokarz for help with the data reduction, and D. Burstein, D. Hanes, R. Kraft, S. Faber, K. Janes, and G. Smith for enlightening conversations.

APPENDIX

Figure 7 shows the DDO colors, C3841, C3842, C4142, and C4245, plotted against [Fe/H] for Galactic globular clusters. The DDO colors are taken from McClure and van den Burgh (1968) and are not corrected for reddening. The values of [Fe/H] are from Zinn and West (1984). Open circles are clusters for which the errors, as quoted by McClure and van den Bergh are 0.10 or more. These points have been excluded from the index-metallicity relations given in Table 10. C3841 and C3842 measure the Fraunhofer line blanketing discontinuity, C4245 measures the strength of the G band, and C4142 is a measure of the cyanogen feature whose bandhead is at ~4215 Å. Despite the lack of a reddening correction, C3841, C3842, and C4245 correlated well with [Fe/H], although less well and with more scatter than the best primary spectroscopic indicators described in this paper.

Also given in Table 10 are the index-metallicity relations for the calibrating M31 clusters plus NGC 188. In this case the DDO

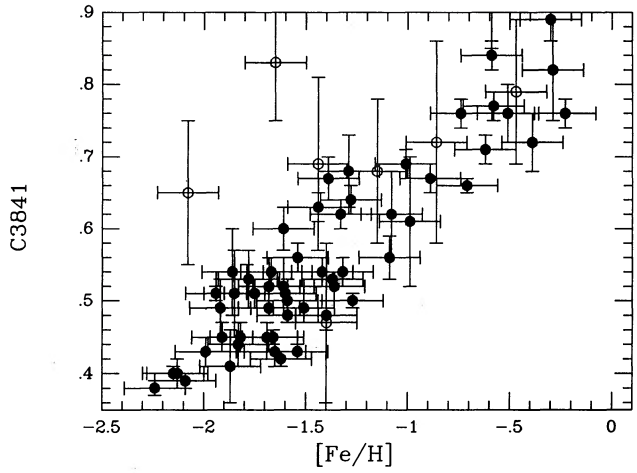

FIG. 7a

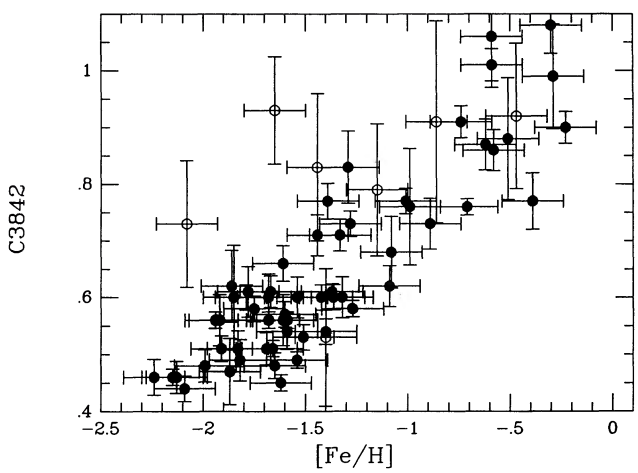

FIG. 7b

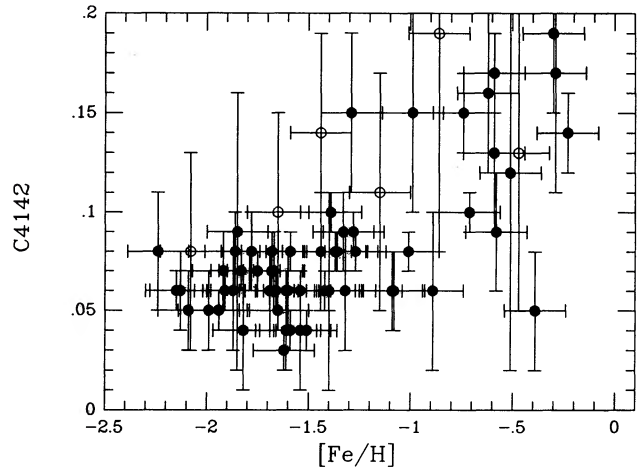

FIG. 7c

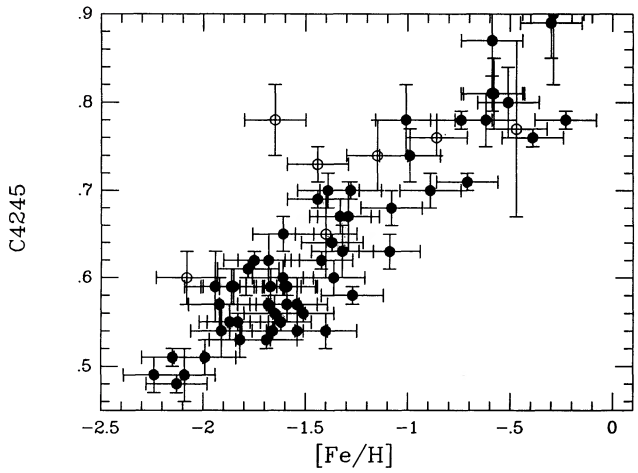

FIG. 7d

FIG. 7.—DDO indices from McClure and van den Bergh (1968) vs. [Fe/H] from Zinn and West (1984) for Galactic globulars. (*a*) C3841, (*b*) C3842, (*c*) C4142, (*d*) C4245.

indices are the pseudocolors measured from the integrated spectra. Except for C4142, the correlations for the Andromeda clusters are substantially worse than for the Galactic globulars. Problems with the spectrophotometry and variations in the cluster reddenings would both be expected to increase the scatter in the M31 cluster relations. However, the lack of scatter in the Δ relation for the same clusters argues against a severe spectroscopic effect, and, for these low-reddening clusters, variations in $E(B-V)$ cannot account for the degree of scatter observed. Interestingly, though, the cyanogen index is more tightly correlated in the M31 sample than in the Galactic sample.

Pseudo–DDO colors were not available for the Galactic globulars, so the further investigation of these results will require additional observations.

TABLE 10

REGRESSIONS OF DDO INDEX AND [Fe/H]

Index	Sample	r	a	b	$\sigma_{[Fe/H]}$	σ_M
C3842.....	GG	0.89	3.22	−3.47	0.25	0.077
	And+188	0.74	1.85	−2.04	0.39	0.210
C3841.....	GG	0.90	3.95	−3.63	0.24	0.059
	And+188	0.69	2.38	−2.17	0.44	0.183
C4245.....	GG	0.92	4.94	−4.53	0.21	0.043
	And+188	0.88	3.79	−1.92	0.27	0.071
C4142.....	GG	0.68	15.00	−2.60	0.43	0.029
	And+188	0.84	7.74	−1.54	0.30	0.039

REFERENCES

Aaronson, M., Cohen, J., Mould, J., and Malkan, M. 1978, *Ap. J.*, **233**, 823.
Armandroff, T. 1989, *A.J.*, **97**, 375.
Battistini, P., Bonoli, F., Braccesi, A., Fusi Pecci, F., Malagnini, M., and Marano, B. 1980, *Astr. Ap. Suppl.*, **42**, 357.
Binggeli, B., Sandage, A., and Tammann, G. 1985, *A.J.*, **90**, 1681.
Bonoli, F., Delpino, F., Federici, F., and Fusi Pecci, F. 1987, *Astr. Ap.*, **185**, 25.
Brodie, J., and Hanes, D. 1986, *Ap. J.*, **300**, 258.
Brodie, J. and Huchra, J. 1990, in preparation.
Burstein, D., Faber, S., Gaskell, M., and Krumm, N. 1981, in *IAU Colloquium 68, Astrophysical Parameters for Globular Clusters*, ed. A. G. D. Philip and D. S. Hayes. (Schenectady: Davis), p. 441.
———. 1984, *Ap. J.*, **287**, 586 (BFGK).
Caldwell, N. 1983, *A.J.*, **88**, 804.
Cohen, J. G. 1981, in *IAU Colloquium 68, Astrophysical Parameters for Globular Clusters*, ed. A. G. D. Philip and D. S. Hayes (Schenectady: Davis), p. 229.
———. 1988, private communication.
Christian, C., and Schommer, R. 1983, *Ap. J.*, **275**, 92.
Cromwell, R., and Weymann, R. 1982, private communication.
Faber, S. 1973, *Ap. J.*, **179**, 731.
Frogel, J., Persson, E., and Cohen, J. 1980, *Ap. J.*, **240**, 785 (FPC).
Harris, W. E. 1988, in *The Extragalactic Distance Scale*, ed. S. van den Bergh and C. Pritchet (Provo: Brigham Young), p. 231.
Hoaglin, D., Mosteller, F., and Tukey, J. 1983, *Understanding Robust and Exploratory Data Analysis* (New York: Wiley).
Huchra, J., Brodie, J. and Stauffer, J. 1991, *Ap. J. Suppl.*, in preparation (HBS).
Huchra, J., Stauffer, J., and van Speybroeck, L. 1982, *Ap. J. (Letters)*, **259**, L57.
Janes, K. 1979, *Ap. J. Suppl.*, **39**, 135.
Latham, D. 1982, in *Instrumentation for Astronomy with Large Optical Telescopes*, ed. C. M. Humphries (Dordrecht: Reidel), p. 259.
Li, G. 1985, in *Exploring Data Tables, Trends and Shapes*, ed. D. Hoaglin, F. Mosteller, and J. Tukey (New York: Wiley), p. 281.
McClure, R. 1970, *A.J.*, **75**, 41.
McClure, R., and van den Bergh, S. 1968, *A.J.*, **73**, 313.
Norris, J. 1978, in *Globular Clusters*, ed. D. Hanes and B. Madore (Cambridge: Cambridge University Press), p. 113.
Rabin, D. 1982, *Ap. J.*, **261**, 85.
Sandage, A. 1962, *Ap. J.*, **135**, 333.
Sargent, W. L. W., Kowal, C., Hartwick, F. D. A., and van den Bergh, S. 1977, *A.J.*, **82**, 947.
Searle, L., Wilkinson, A., and Bagnuolo, W. 1980, *Ap. J.*, **261**, 85.
Smith, G. H. 1987, *Pub. A.S.P.*, **99**, 67.
Suntzeff, N. 1980, *A.J.*, **85**, 408.
———. 1981, *Ap. J. Suppl.*, **47**, 1.
Tripicco, M. J. 1989, *A.J.*, **97**, 735.
Zinn, R. 1980*a*, *Ap. J. Suppl.*, **42**, 19.
———. 1980*b*, *Ap. J.*, **241**, 602.
Zinn, R., and West, M. 1984, *Ap. J. Suppl.*, **55**, 45.

JEAN P. BRODIE: Lick Observatory, University of California, Santa Cruz, CA 95064

JOHN P. HUCHRA: Center for Astrophysics, 60 Garden Street, Cambridge, MA 02138